To appear in AGU Monograph "Planetary Magnetotails" in 2014.

PHYSICS OF COMETARY MAGNETOSPHERES

Tamas I. Gombosi[1]

This tutorial summarizes our present, pre-Rosetta understanding of the basic physical processes operating in cometary environments with particular attention to cometary magnetotails. Ionization of cometary gases is responsible for most plasma processes in the magnetospheres of active comets. The interaction between the superalfvénic, magnetized solar wind and cometary ions forms a number of plasma boundaries starting with the weak bow shock and continuing with the contact surface (diamagnetic cavity boundary), the recombination layer and the inner shock. The plasma tail is sensitive to changes in the solar wind and to varying cometary activity. These processes will be explored in detail.

1. INTRODUCTION

Our present understanding of cometary atmospheres is based on Whipples "dirty iceball" idea in which the nucleus consists of a mixture of frozen volatiles and nonvolatile dust [*Whipple*, 1950]. Figure 1 shows images of all cometary nuclei photographed by spacecraft so far.

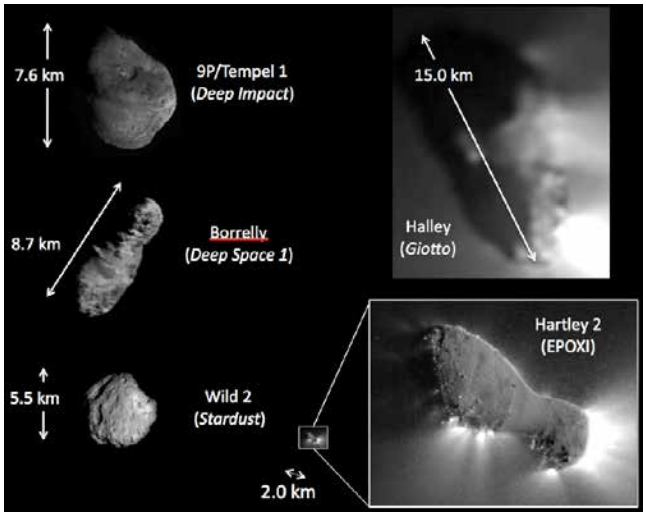

Figure 1. Cometary nuclei visited by spacecraft prior to the Rosetta mission (credit: Michael A'Hearn, EPOXI team/University of Maryland/JPL/NASA.

As cometary nuclei approach the sun, water vapor and other volatile gases sublimate from the surface layers generating a rapidly expanding cloud of dust and gas. The freshly sublimated gas leaves the surface at slightly less than the local speed of sound, it undergoes a sonic transition near the surface and it propagates as a "cometary wind" into interplanetary space. The sublimating gases are capable of blowing away specks of dust from the surface [cf. *Mendis et al.*, 1985; *Gombosi et al.*, 1986; *Tenishev et al.*, 2008; *Zakharov et al.*, 2009].

It was recognized a long time ago that the expanding cometary exosphere represents an extensive, "soft" obstacle for the supersonic and super-Alfvénic solar wind flow [*Biermann et al.*, 1967]. The resulting interaction is very different from that with other solar system bodies with gravitationally bound dense atmospheres and/or significant intrinsic magnetic fields. Neutral atoms and molecules of cometary origin become ionized (because of photoionization, charge transfer or electron impact ionization) with characteristic ionization scale lengths of $10^5 - 10^7$ km. The ionization process introduces a new, practically stationary particle into the high speed magnetized flow of the solar wind. Spacecraft instrumentation at comets detected large amplitude low frequency magnetic field fluctuations. These fluctuations grow from the relatively low solar wind turbulence level (at large cometocentric distances) to very large amplitudes near the comet. The enhanced fluctuation level is due to instabilities associated with "mass loading," due to the interaction of the solar wind with the newly ionized cometary material.

In their pioneering work *Biermann et al.* [1967] predicted that the deceleration of the solar wind flow by mass loading leads to the gradual deceleration of the solar wind flow at large cometocentric distances and eventually to the formation of a weak shock ($M \approx 2$) where the flow is impulsively decelerated to subsonic velocities. This was a revolutionary idea, since it predicted that

[1]Department of Atmospheric, Oceanic and Space Sciences, University of Michigan, 2428 Space Research Building, Ann Arbor, MI 48109, USA.

the presence of the comet can be "felt" far upstream from the nucleus in the supersonic solar wind flow. Later *Galeev et al.* [1985] recognized that implanted cometary ions carry most of the "thermal" pressure (ie. the second moment of the distribution function) and that charge exchange cooling of the implanted plasma population can play a very important role in the dynamics of the contaminated solar wind flow. Their model predicted a weak and highly structured shock with a viscous subshock, a continuously decelerated and cooled plasma flow behind the shock and finally a stagnation region. *In situ* measurements later confirmed the gross features predicted by this model [cf. *Gringauz et al.*, 1986; *Johnstone et al.*, 1986; *Neubauer et al.*, 1986].

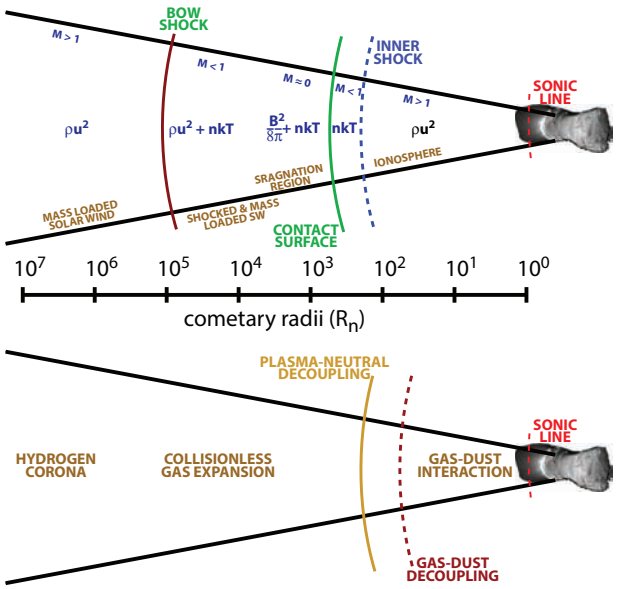

Figure 2. Schematic representation of the plasma (upper panel) and neutral gas (lower panel) environment of an active comet [after *Gombosi et al.*, 1986].

Downstream of the bow shock the plasma population is a varying mixture of shocked plasma (solar wind contaminated with upstream pick-up particles) and cometary plasma ionized in the subsonic region. This region is called the cometosheath. The cometosheath is characterized by a rapidly increasing rate of ion pickup (as the plasma moves towards the comet), resulting in continuous deceleration (and eventual stagnation) of the plasma flow, accompanied by increasing plasma density and magnetic field magnitude [*Balsiger et al.*, 1986; *Neubauer et al.*, 1986]. The inner, nearly stagnating region of the cometosheath is primarily photochemically controlled and the plasma density varies with the inverse of the cometocentric distance [cf. *Balsiger et al.*, 1986].

In the innermost region of the cometary environment the plasma is of cometary origin and it is strongly coupled to the outflowing neutral atmosphere. This part of the coma is called the "cometary ionosphere" and it is magnetic field free, since the heavily mass loaded solar wind plasma cannot penetrate into this region [cf. *Neubauer et al.*, 1986; *Balsiger et al.*, 1986]. A schematic view of the dayside cometary atmosphere is shown in Figure 2.

Our understanding of the main physical processes controlling the "ionopause" (the surface separating the magnetized cometosheath plasma from the magnetic field-free inner cometary ionosphere) was significantly modified by Giotto's encounter with comet Halley. A diamagnetic cavity boundary is formed at a location where the inward-pointing (towards the comet) total magnetic force (the sum of the magnetic pressure gradient and magnetic curvature forces) is balanced by the outward pointing ion-neutral drag force. Before the cometary encounters, an inner shock was predicted inside the "ionopause" to decelerate the supersonic outflow of the cometary ions and divert them toward the tail. In reality, the drag by the rapidly expanding neutral gas forces the plasma to maintain supersonic velocity up to the immediate vicinity of the diamagnetic cavity boundary, where it undergoes a shock transition [*Cravens*, 1989; *Goldstein et al.*, 1989]. The shocked ionospheric plasma piles up, and is rapidly removed by recombination.

Comets exhibit two distinct types of tails. A nice example is comet Hale-Bopp that is shown in Figure 3.

Figure 3. Comet Hale-Bopp (1997) showing two distinct tails – a dust tail (white) and an ion tail (blue) (source: http://www.tivas.org.uk/solsys/tas_solsys_comet.html)

For active comets the straight, narrow plasma tails (also called Type I tails) are $10^7 - 10^8$ km long and, within a few degrees, always point away from the sun. This observation inspired *Biermann* [1951] to postulate the existence of a continuous "solar corpuscular radiation" (solar wind). Assuming that the antisunward acceleration of small irregularities in Type I comet tails were due to collisional coupling between a radially outward plasma flow from the Sun and newly ionized cometary particles *Biermann* [1951] inferred a solar wind density and velocity of $n_{sw} \approx 1,000$ cm^{-3} and $u_{sw} \approx 1,000$ km/s that represents a particle flux ∼500 times larger than was later observed.

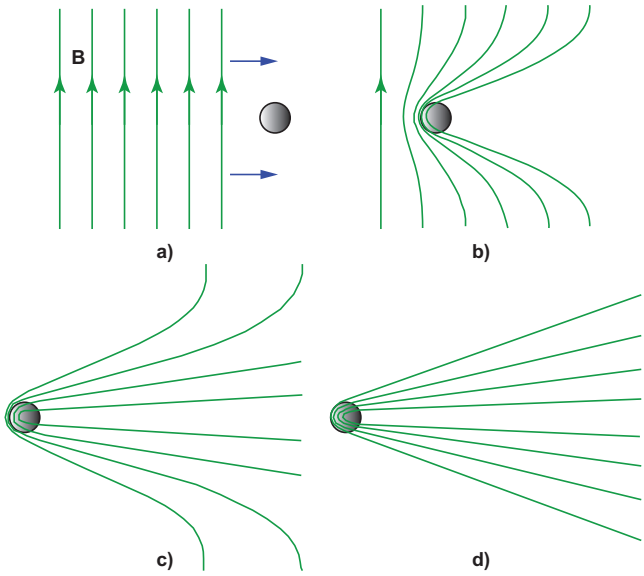

Figure 4. Alfvén's scenario of the formation of comet tails. A plasma beam with a frozen-in magnetic field approaches the head of a comet (panel a); the field is deformed (panels b and c); the final state is reached when the beam has passed (panel d) [*Alfvén*, 1957].

A few years later *Alfvén* [1957] pointed out that the plasma densities inferred by *Biermann* [1951] were inconsistent with observed coronal densities (assuming that the plasma density decreases with the square of the heliocentric distance as the solar corpuscular radiation moves outward). *Alfvén* [1957] offered an alternative explanation for the formation of cometary plasma tails that is depicted in Figure 4. The main assumption in this model was that the solar corpuscular radiation was carrying a "frozen-in" magnetic field that "hangs up" in the high density inner coma where the solar particles strongly interact with the cometary atmosphere and consequently the solar plasma flow considerably slows down. This interaction results in a "folding" of the magnetic field around the cometary coma that creates the long plasma tail. Disturbances along the folded magnetic field lines propagate as magnetohydrodynamic waves and they can reach velocities of 100 km/s even if the solar plasma has a density of ~ 5 cm^{-3}.

The second type of tails are broad and curved dust tails (also called Type II tails) that usually lag behind the Sun-comet line (opposite to the direction of cometary orbital motion). Since the gravity of the cometary nucleus is negligible, the motion of the dust particles is controlled by an interplay between solar gravity and solar radiation pressure. Assuming that dust grains have a more or less constant mass density, ρ_d, the antisunward radiation pressure, F_{rad} is inversely proportional to the square of the heliocentric distance, d_h, and proportional to the cross section of the dust grain, πa^2 (a is the equivalent radius of a spherical dust grain), $F_{rad} \propto a^2/d_h^2$. The sunward pointing gravitational force is proportional to the particle mass ($4\pi\rho_d a^3/3$) and inversely proportional to the heliocentric distance: $F_{grav} \propto a^3/d_h^2$. Since the two forces point in the opposite direction and have the same heliocentric dependence, but exhibit different dependence on the grain size ($F_{rad} \propto a^2$ and $F_{grav} \propto a^3$) the resulting effect is a complex "dust mass spectrometer" where each particle size is moving under the influence of its own "reduced solar gravity." This effect results in the broad and curved dust tail.

2. THE COMA

2.1. Gas Production

The atmospheres of comets, commonly referred to as comas, are different in a number of important ways from planetary atmospheres. The most important distinguishing characteristics of comas are (1) the lack of any significant gravitational force, (2) relatively fast radial outflow velocities, and (3) the time-dependent nature of their physical properties. A direct consequence of these features is the expanding nature of cometary atmospheres.

The source of cometary activity is the sublimation of cometary volatiles. There are many sophisticated sublimation models (for a nice review we refer to *Davidsson* [2008]), but the basic concept is well illustrated by the classic *Delsemme and Swings* [1952] theory who considered a cometary nucleus covered by a homogeneous surface of sublimating water ice. They assumed that the surface did not contain macroscopic irregularities; i.e., surface irregularities were much smaller than the mean free path of vaporized particles. As the pressure of the cometary atmosphere is much smaller at the nucleus surface than the critical pressure of the phase transition triple point, the liquid phase is unstable and sublimation of frozen volatiles is responsible for gas production. Assuming that the

sublimated gas was in equilibrium with the surface, *Delsemme and Swings* [1952] applied the Clausius-Clapeyron equation to determine the steady state saturated gas pressure:

$$p_s\left(T_s\right) = p_r \exp\left[\frac{L\left(T_s\right)}{kN_A}\left(\frac{1}{T_r} - \frac{1}{T_s}\right)\right] \qquad (1)$$

where T_s is the surface temperature, p_s is the vapor pressure, p_r is the saturated vapor pressure at a reference temperature, T_r, $L(T_s)$ is the latent heat of vaporization, k is the Boltzmann constant and N_A is Avogadro's number. For water ice the latent heat is fairly insensitive to temperature and it can be approximated by a value of $L_w = 4.80 \times 10^4$ joule/mol [*Delsemme and Miller*, 1971]. The sublimation vapor pressure of boiling water is $p_r = 10^5$ Pa at $T_r = 373$ K.

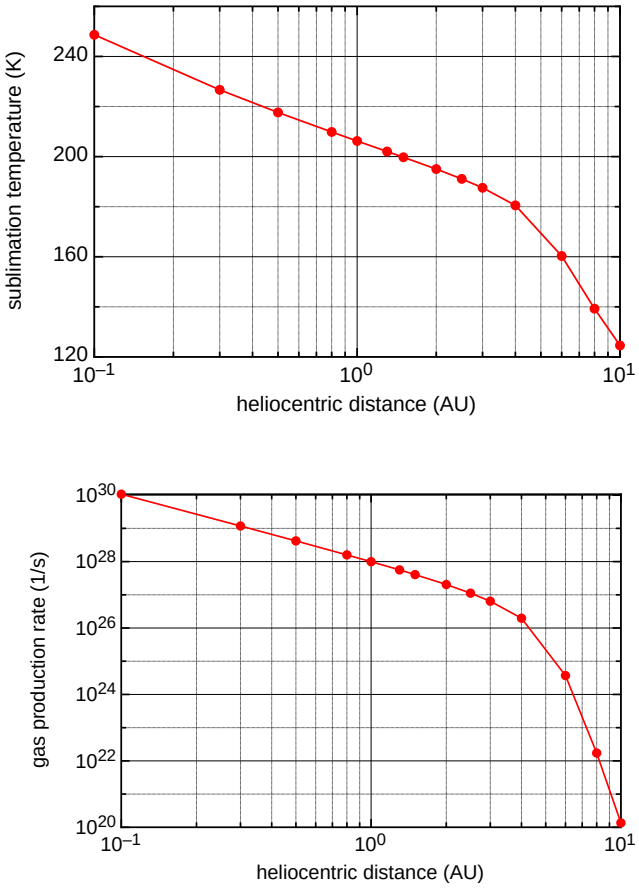

Figure 5. Sublimation temperature (upper panel) and gas production rate (lower panel) of a "*Delsemme and Swings* [1952] type" comet with 1 km radius, assuming that only 5% of subsolar area is active.

Delsemme and Swings [1952] also assumed that the sublimated molecules behave as a perfect gas ($p_s = n_s k T_s$), thus defining the gas number density, n_s, just above the surface. In addition, they considered a low-pressure kinetic model and calculated the flux of scattered gas particles moving away from the nucleus:

$$\dot{z}\left(T_s\right) = \frac{1}{4} n_s u_{th} = n_s\left(T_s\right)\sqrt{\frac{kT_s}{2\pi m_c}} \qquad (2)$$

Here m_c is the mass of a cometary volatile molecule (in our case $m_c = 18$ amu) and u_{th} is the thermal speed of the gas ($u_{th} = \sqrt{8kT_s/\pi m_c}$).

In the simplest scenario one can assume that the incident solar energy flux is balanced by black body radiation and sublimation:

$$\frac{J_{sol}}{d_h^2} = \dot{z}\left(T_s\right)\frac{L_w}{N_A} + \sigma_{SB} T_s^4 \qquad (3)$$

where $J_{sol} = 1365$ W is the solar radiation energy flux at 1 AU and σ_{SB} is the Stefan-Boltzmann constant. We note that in equation (3) the heliocentric distance is measured in units of AU. Figure 5 shows the sublimation temperature (upper panel) and gas production rate (lower panel) obtained by solving equations (1) through (3) for an iceball with radius of 1 km. It was also assumed that only about 5% of the surface area is active at any given time [cf. *Combi et al.*, 2012]. The "effective" sublimating surface can be significantly increased by grain sublimation in the coma. This process is able to increase the apparent sublimating area by a large factor [*Fougere et al.*, 2013].

Inspection of Figure 5 reveals that water production "turns on" around 3.5 AU. It reaches about 10^{28} s^{-1} near 1 AU and a spectacular 10^{30} s^{-1} for a sun-grazing comet. The collisional mean free path near the surface of active comets is less than a meter, therefore the gas rapidly engulfs the nucleus, even though only a small fraction of the surface area is active. In a first approximation spherically symmetric gas coma models provide reasonable results for most comets [cf. *Zakharov et al.*, 2009; *Combi et al.*, 2012].

2.2. Ion-Neutral Coupling

Here we present a very simple, spherically symmetric description of the innermost region of active comet atmospheres that captures most of the basic physics without going into too much detail. This description follows the derivation of *Cravens* [1989] and it is a nice tool for a tutorial. However, those who are interested in more details are referred to appropriate review papers [cf. *Strobel*, 2002; *Rubin et al.*, 2011].

The neutral composition in the inner coma is assumed to be pure water and for cometocentric distances much larger than a few times the radius of the nucleus but much smaller than the ionization scale-length ($\lambda \approx 10^6$ km), the neutral density is given by

$$n_n = \frac{Q}{4\pi u_n r^2} \qquad (4)$$

where Q is the total gas production rate of the comet and $u_n \approx 1$ km/s is the radial outward velocity of neutral water molecules. Expression (4) neglects the exponential decrease of the neutral density on scales of the ionization length (λ), but here we are describing a region much smaller than λ.

The primary photoionization products are H_2O^+ and OH^+, but the dominant ion in the collisional inner comas is H_3O^+ that is rapidly formed by the

$$H_2O^+ + H_2O \rightarrow H_3O^+ + OH \tag{5}$$

reaction [cf. *Mendis et al.*, 1985]. The production rate of cometary ions is dominated by photoionization and it can be approximated as

$$S_i = \frac{I_0}{d_h^2} n_n \tag{6}$$

where $I_0 \approx 10^{-6}$ s^{-1} is the ionization frequency at 1 AU [*Cravens*, 1989]. The H_3O^+ ions are destroyed by dissociative recombination that produces a neutral water molecule and a hydrogen atom. The reaction rate coefficient of this dissociative recombination is dependent on the electron temperature: $\alpha = 1.21 \times 10^{-5}/\sqrt{T_e}$ cm^3/s resulting in an ion loss rate of $L_i = \alpha n_i^2$ (assuming that the ion and electron densities are equal) [cf. *Mendis et al.*, 1985]. This expression for the recombination rate is valid below approximately 800 K [cf. *Schunk and Nagy*, 2000; *Rubin et al.*, 2014].

The continuity and momentum equations for the radially expanding unmagnetized ionosphere near the nucleus can be written as

$$\frac{\partial n_i}{\partial t} + \frac{1}{r^2}\frac{\partial}{\partial r}\left(r^2 u_i n_i\right) = \frac{I_0}{d_h^2} n_n - \alpha n_i^2 \tag{7}$$

and

$$m_i n_i \frac{\partial u_i}{\partial t} + m_i n_i u_i \frac{\partial u_i}{\partial r} + \frac{\partial p_i}{\partial r} = \left(m_i n_i \nu_{in} + \frac{I_0}{d_h^2} m_n n_n\right)(u_n - u_i) \tag{8}$$

where n_i and p_i are the density and pressure of H_3O^+ ions, $m_n = 18$ amu, $m_i = 19$ amu, and $\nu_{in} = k_{in} n_n$ is the ion-neutral charge transfer collision frequency ($k_{in} = 1.1 \times 10^{-9}$ cm^3/s) [*Cravens and Körösmezey*, 1986]. The right hand side of equation (8) describes the ion-neutral momentum coupling due to charge exchange (first term) and the production of new ions from neutrals (second term).

Quite a few physical insights can be gained by inspecting equations (7) and (8). Let us first examine the ion-neutral coupling term. For an active comet the ion-neutral coupling time scale can be approximated by

$$\tau_{in} \approx \frac{4\pi u_n r^2}{k_{in} Q} \tag{9}$$

As long as the coupling time is shorter than the characteristic transport time, $\tau_{transp} = r/u_n$, the ions and neutral velocities remain closely coupled and in a good approximation $u_i \approx u_n$. The radial distance where $\tau_{in} = \tau_{transp}$ is the distance where the ions decouple from the neutrals in the absence of any other process (note that so far we completely neglected the interaction of the cometary coma with the solar wind):

$$R_{in} \approx \frac{k_{in} Q}{4\pi u_n^2} = 875 \left(\frac{Q}{10^{28}}\right) \quad \text{[km]} \tag{10}$$

For a Halley class comet ($Q \approx 7 \times 10^{29}$) we get $R_{in} \approx 6 \times 10^4$ km, while for a typical active comet ($Q \approx 10^{28}$) we get $R_{in} \approx 900$ km. It should be mentioned again, that the solar wind interaction might push other plasma boundaries inside this region, so the strongly coupled ionospheric plasma might not extend to this distance.

It is obvious from the above discussion that in the cometary ionosphere the ions are closely coupled to the neutrals and the ion velocity is very close to the neutral velocity, $u_i \approx u_n$. Since the neutral velocity is more or less constant, we conclude that in the ionosphere the ion velocity is also constant. This makes it possible to evaluate the radial profile of the ion density using the continuity equation (equation 7).

Substituting the constant neutral velocity for the ion velocity and considering steady state conditions the continuity equation becomes the following:

$$\frac{\partial}{\partial r}\left(r^2 n_i\right) = \frac{I_0}{d_h^2}\frac{Q}{4\pi u_n^2} - \frac{\alpha}{u_n} r^2 n_i^2 \tag{11}$$

It is obvious that the solution to equation (11) is $n_i \propto r^{-1}$:

$$n_i = \left[\sqrt{1 + \frac{Q}{Q_0}} - 1\right]\left(\frac{u_n}{2\alpha}\right)\frac{1}{r} \tag{12}$$

where

$$Q_0 = \frac{\pi d_h^2 u_n^3}{\alpha I_0} \approx 2.6 \times 10^{26}\, d_h^2 \sqrt{T_e} \tag{13}$$

For active comets $Q \gg Q_0$ and therefore

$$n_i \approx \sqrt{\frac{Q}{Q_0}}\left(\frac{u_n}{2\alpha}\right)\frac{1}{r} \tag{14}$$

When deriving equation (12) we assumed that the radial dependence of the recombination rate coefficient can be neglected. For a typical active comet ($R_n \approx 1$ km, $Q \approx 10^{28}$ s^{-1}) we get about $n_n \approx 10^{12}$ cm^{-3} and $n_i \approx 10^7$ cm^{-3} at the surface.

A word of caution is in order at this point. In the immediate vicinity of the nucleus the fluid approximation is not valid and a thin kinetic "Knudsen layer" separates the nucleus from the collisional coma. Expressions (12) and (14) were obtained in the fluid approximation, so they are not strictly valid inside the Knudsen layer.

2.3. Inner Shock and Contact Surface

The radially outward flowing cometary ionosphere is separated from the heavily contaminated and nearly stagnating outside plasma by a tangential discontinuity, the contact surface (sometimes also called diamagnetic cavity boundary). For active comets this contact surface is located deep inside the region where ion-neutral collisions force the cometary ionosphere to expand with the velocity of the neutral gas (see Section 2.2). Outside the contact surface the magnetic field "piles up" due to the very small plasma flow velocity.

There are two physical constraints that control the location of the contact surface: the balance between the ambient solar wind pressure and the outward ion-neutral drag, and the recombination rate coefficient that is a function of electron temperature.

2.3.1. Electron Temperature

Let us start with the electron temperature. Deep in the collisional coma inelastic collisions between the thermal electrons and the neutral water molecules result in rotational and vibrational excitation of the molecule; the rate for this interaction is especially large because of the polar nature of the water molecule. The electron-neutral collision frequency can be approximated by [*Banks and Kockarts*, 1973]:

$$\nu_{en} = 2.615 \times 10^{-5} \frac{n_n}{\sqrt{T_e}} \qquad (15)$$

where the collision frequency is given in Hz and n_n is given in units of cm^{-3}. The characteristic time-scale of electron-neutral collisions is

$$\tau_{en} = 4.81 \times 10^{-3} \sqrt{T_e} \frac{10^{28}}{Q} \frac{r^2}{R_n^2} \quad \text{s} \qquad (16)$$

Electrons and neutrals remain closely coupled as long as τ_{en} is smaller than the dynamical timescale of the expanding ionospheric plasma, $\tau_{transp} = r/u_n$. This condition yields the electron-neutral decoupling distance, where the electron temperature exhibits a sharp, nearly two orders of magnitude increase [*Körösmezey et al.*, 1987]. The ratio of the electron-neutral decoupling distance to the nucleus radius is now

$$\frac{R_{en}}{R_n} = \frac{208}{\sqrt{T_e}} \frac{Q}{10^{28}} \frac{R_n}{u_n} \qquad (17)$$

Typical electron temperatures in the collisional coma are $\approx$ 100 K. For a Halley class comet ($Q \approx 7 \times 10^{29}$, $R_n = 7$ km) we get $R_{en} \approx 7 \times 10^4$ km, while for a typical active comet ($Q \approx 10^{28}$, $R_n = 1$ km) the decoupling radius is $R_{en} \approx 20$ km.

In considering the thermal coupling and the electron temperature, more relevant than the elastic electron-neutral collisions is the electron-neutral water cooling process, which is dominated in the inner coma by rotational cooling [cf. *Körösmezey et al.*, 1987; *Schunk and Nagy*, 2000]. Recently, Cravens (private communication 2013) derived an an analytic expression that fits the sum of the rotational, vibrational, and electronic cooling cooling rates for the temperature interval of $kT_n \le kT_e \le 0.8$ eV ($T_e \approx 9,300$ K) with about 5% accuracy. The functional form of the electron cooling rate, L_e, is based on the tabulated results of *Gan and Cravens* [1990] and *Cravens et al.* [2011]:

$$L_e = A_1 \left[1 - \exp\left(-\frac{k(T_e - T_n)}{0.033\text{eV}}\right)\right] + A_2 \left[0.415 - \exp\left(-\frac{kT_e - 0.10\text{eV}}{0.10\text{eV}}\right)\right] \qquad (18)$$

where $A_1 = 4 \times 10^{-9}$ eV cm^3 s^{-1}, $A_2 = 0$ for $kT_e \le 0.188$ eV and $A_2 = 6.5 \times 10^{-9}$ eV cm^3 s^{-1} for $kT_e > 0.188$ eV.

The electron cooling time-scale on water can now be expressed as

$$\tau_{ew} = \frac{kT_e}{n_n L} = \frac{kT_e}{L} \frac{4\pi u_n r^2}{Q} \qquad (19)$$

In the collision dominated region $T_e \approx T_n$ and we define the characteristic cooling time for an electron temperature that is only 1 K above the neutral temperature. This yields a numerical value for the quantity kT_e/L:

$$\tau_{ew} = 2.1 \times 10^{-3}\, r^2 \left(\frac{u_n}{1\,\text{km/s}}\right) \left(\frac{10^{28}\,\text{s}^{-1}}{Q}\right) \qquad (20)$$

where r is measured in kilometers.

The electron temperature will decouple from the ion temperature near the point where electron cooling time-scale and the plasma dynamical timescale, $\tau_{transp} = r/u_n$, are about equal:

$$R_{ew} = 480 \left(\frac{1\,\text{km}^2/\text{s}^2}{u_n^2}\right) \left(\frac{Q}{10^{28}\,\text{s}^{-1}}\right) \qquad (21)$$

where R_{ew} is given in kilometers. For a Halley class comet ($Q \approx 7 \times 10^{29}$) we get $R_{ew} \approx 3.4 \times 10^4$ km, and for a weak comet ($Q \approx 10^{28}$) the water cooling decoupling distance is about 500 km.

2.3.2. Inner Shock

The ion-acoustic speed of the collisional ionospheric plasma is $\approx$ 0.35 km/s, so the expand-

ing plasma flow inside the contact surface is supersonic. However, this radially expanding supersonic plasma flow cannot continue beyond the contact surface that separates the cometary ionosphere from the contaminated solar wind plasma. Since a supersonic flow cannot "turn" it has to be terminated by an "inner shock" before it reaches the contact surface. On the dayside the shocked, subsonic flow nearly stagnates before it is gradually diverted towards the tail.

The ion density between the inner shock and the contact surface, however, is not determined by the local photochemical equilibrium, because plasma is continuously supplied from the expanding ionosphere [*Cravens*, 1989]. This plasma is lost by recombination. The balance between supply and loss can be expressed as

$$\alpha n_{rec}^2 \Delta = n_i u_n \tag{22}$$

where Δ is the thickness of the recombination layer between the shock and the contact surface and $n_{rec} \approx 4n_i$ is the ion density in the recombination layer (this assumes a strong hydrodynamic shock). This equation can be solved for Δ:

$$\Delta \approx \frac{1}{8}\sqrt{\frac{Q_0}{Q}} R_{cs} \tag{23}$$

where R_{cs} is the cometocentric distance of the contact surface.

For active comets the thickness of the recombination layer is very small compared to R_{cs}. For instance, in the case of comet Halley, Δ was so small that special data analysis was needed to identify the associated density peak. Figure 6 shows the comparison of a global MHD simulation with Giotto observations for the H_3O^+ hydronium ion with mass/charge of 19 amu/e [*Rubin et al.*, 2009]. H_3O^+ is the dominant ion within 30,000 km of Comet 1P/Halley's nucleus. Outside 40,000 km the experimental data can be well fitted by a higher production rate curve, indicating strong time dependence of the cometary gas production.

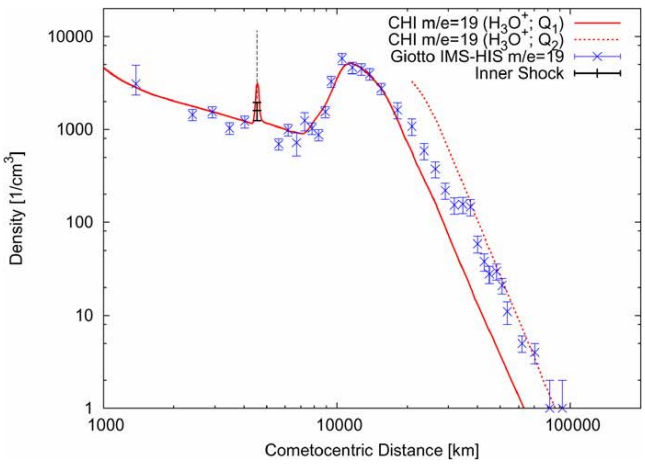

· **Figure 6.** Mass/charge = 19 amu/e density profile including the H_3O^+ ion along the Giotto trajectory compared to the Giotto IMS data from the HIS sensor (points). The position of the inner shock is also given, indicated by the mean (measured over one 4 s spin period of Giotto) as well as the maximum density (dashed vertical line; density measured during a fraction of a spin period). The observations are compared to simulation results obtained with two different production rates, Q_a and Q_2 [*Rubin et al.*, 2009]

Giotto's Ion Mass Spectrometer (IMS) performed continuous measurements, scanning in 1/4 s through $m/e = 12 - 57$ amu/e in 64 steps with 1/256 s accumulation time each. During a spin period of 4 s therefore IMS acquired 16 mass spectra including a whole mass scan each. Inside 40,000 km the data is averaged over the whole period and outside this distance over five spin periods. During a fraction of a spin period the Giotto IMS measured a distinct rise in count rate at a cometocentric distance of roughly 4550 km. *Goldstein et al.* [1989] and *Cravens* [1989] identified the sharp spike (about 47 km in width) as coming from the recombination layer between the inner shock and the contact surface.

Inspection of Figure 6 also shows that the plasma density in the inner cometary atmosphere decreases as r^{-1}, as predicted by equation (14). The narrow cavity boundary region (with the contact surface and inner shock) was at around 4550 km. The electron-neutral decoupling took place around 2×10^4 km. Beyond this boundary the plasma density decreases as r^{-2}, because recombination is no longer important. Qualitatively similar simulation results were obtained earlier by *Gombosi et al.* [1996], *Häberli et al.* [1997] and *Benna and Mahaffy* [2007].

Looking forward to comet Churyumov-Gerasimenko it needs to be pointed out that in the case of weak comets *Delta* ≈ 0.1 and therefore finite gyroradius effects will come into play. In this case, at least for determining some of the structure, a hybrid simulation would be helpful [e.g. *Puhl-Quinn and Cravens*, 1995].

2.3.3. Contact Surface

At the contact surface the outside $j \times B$ force is balanced on the inside by the ion-neutral drag force [*Cravens*, 1986; *Ip and Axford*, 1987]:

$$\nabla \frac{B^2}{2\mu_0} - \left(\frac{\mathbf{B}}{\mu_0} \cdot \nabla\right) \mathbf{B} = (m_i n_i \nu_{in}) (\mathbf{u}_n - \mathbf{u}_i) \tag{24}$$

where μ_0 is the magnetic permeability of free space and for the sake of simplicity we neglected the ionization drag. The first term on the left hand side is the magnetic pressure gradient while the second term describes the magnetic tension force. In the immediate vicinity of the contact surface the pressure gradient force dominates over the magnetic

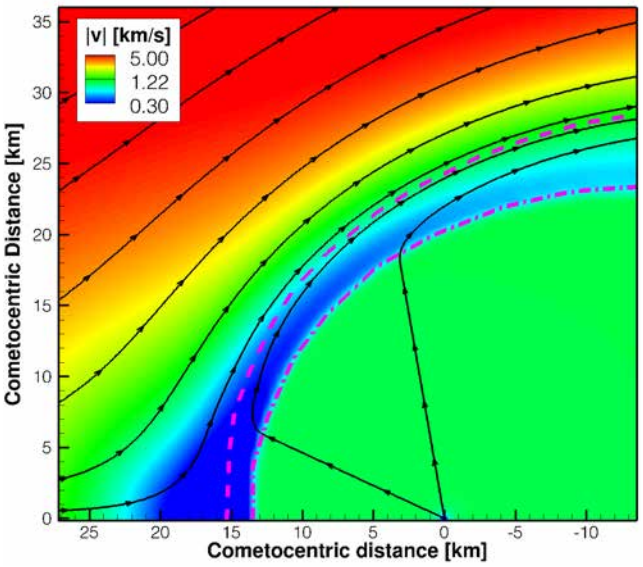

Figure 7. Plasma bulk flow velocity (and streamlines) for comet Churyumov-Gerasimenko with the Sun on the left hand side and the comet centered at the origin. While inside the contact surface (dashed line) the plasma flow is dominated by collisions with the abundant neutrals flowing out radially, outside the inner shock (dash-dot line)) the plasma flow is bent tailward and its flow velocity becomes parallel to the shock increases. [*Rubin et al.*, 2012]

tension force, because this is the region where the "piled up" magnetic field rapidly goes to zero inside the contact surface thus forming the diamagnetic cavity. The maximum value of the magnetic field in the pile-up region is reached at a cometocentric distance of R_{max} and its value can be estimated by equating the magnetic pressure with the dynamic pressure of the ambient solar wind that is driving the entire interaction:

$$m_p n_{sw} u_{sw}^2 = \frac{B_{max}^2}{2\mu_0} \tag{25}$$

where m_p is the proton mass.

Substituting equation (14) into equation (24) and neglecting the magnetic tension term yields the following:

$$\frac{\partial}{\partial r}\left(\frac{B^2}{2\mu_0}\right) = \frac{m_i k_{in}}{4\pi d_h}\sqrt{\frac{I_0}{4\pi\alpha u_n}}\frac{Q^{3/2}}{r^3} \tag{26}$$

Equation (26) can be integrated from the contact surface, R_{cs}, where the magnetic field vanishes to R_{max}, where the magnetic field reaches its maximum value (see equation 25):

$$m_p n_{sw} u_{sw}^2 = A\left(\frac{Q}{10^{28}}\right)^{3/2}\left(\frac{R_n^2}{R_{cs}^2} - \frac{R_n^2}{R_{max}^2}\right) \tag{27}$$

where

$$A = 10^{42}\frac{m_i k_{in}}{4\pi d_h}\sqrt{\frac{I_0}{4\pi\alpha u_n}}\frac{1}{R_n^2} \tag{28}$$

Assuming that $R_{max}^2 \gg R_{cs}^2$ the radius of the contact surface becomes

$$R_{cs} = \sqrt{\frac{m_i}{m_p}\frac{k_{in}}{4\pi d_h n_{sw} u_{sw}^2}\sqrt{\frac{I_0}{4\pi\alpha u_n}}Q^{3/4}} \tag{29}$$

Substituting the numerical values and using typical solar wind parameters ($n_{sw} = 5$ cm^{-3} at 1 AU and $u_{sw} = 400$ km/s) we get

$$R_{cs} = 7.11\times 10^{-20} T_e^{1/4}\sqrt{d_h}\, Q^{3/4} \quad \text{[km]} \tag{30}$$

Assuming $T_e \approx 10^2$ K in the collisional coma for a Halley class comet we get $R_{cs} \approx 5500$ km and for a typical active comet $R_{cs} \approx 225$ km. We note that for a Halley class comet $R_{cs} \ll R_{en}$, while for a typical active type comet $R_{cs} \gg R_{en}$.

Recently *Rubin et al.* [2012] performed large scale MHD simulations for a relatively weak comet (representing comet 67P/Churyumov-Gerasimenko). Figure 7 shows the diamagnetic cavity. The color code represents the magnitude of plasma velocity, while the streamlines show the plasma trajectories. One can see that in the ionosphere the ions are supersonic and moving radially outward with the neutral velocity. The ions are practically stagnating in the recombination region. Outside the contact surface the contaminated solar wind flows around the contact surface.

3. MASS LOADING

A well developed cometary atmosphere extends to distances several orders of magnitude larger than the size of the nucleus. It is the mass loading of the solar wind with newly created cometary ions, from this extended exosphere, that is responsible for the interaction with the solar wind and the formation of cometary magnetotails. Mass loading occurs when a high speed magnetized plasma moves through a background of neutral particles which is continuously ionized. Photoionization and electron impact ionization result in the addition of plasma to the plasma flow, while charge-exchange replaces fast ions with almost stationary ones. "Ion pickup" (or ion implantation) is the process of accommodation (but not thermalization) of a single newborn ion to the plasma flow. The combined effect of the various ionization processes is usually net mass addition. Conservation of momentum and energy requires that the plasma flow be decelerated as newly born charged particles are "picked up." The process of continuous ion pickup and its feedback to the plasma flow is called "mass loading." A detailed review of mass loading in space plasmas can be found in *Szegő et al.* [2000], while *Coates and Jones* [2009] published an excellent summary of the cometary mass loading process.

Freshly born ions are accelerated by the motional electric field of the high-speed solar wind flow. The ion trajectory is cycloidal, resulting from the superposition of gyration and $E \times B$ drift. The corresponding velocity-space distribution is a ring-beam distribution, where the gyration speed of the ring is $u \sin\alpha$, (where u is the bulk plasma speed and α is the angle between the solar wind velocity and magnetic field vectors) and the beam velocity (along the magnetic field line) is $u \cos\alpha$.

The ring beam distribution has large velocity space gradients and it is unstable to the generation of low frequency transverse waves. The ions both gyrate about the magnetic field and $E \times B$ drift, such that the ion trajectories are cycloidal. The ring-beam distribution is highly unstable against the growth of ultra-low frequency (or ULF) electromagnetic waves (i.e., frequencies near the heavy ion gyrofrequency, or ≈10 mHz). The wave spectrum tends to have a strong monochromatic component for less active comets or at large cometocentric distances (i.e., comet Giacobini-Zinner far upstream) but tends to be turbulent-like with power spread over a large range of wavenumbers for regions closer to the comet [*Sagdeev et al.*, 1986; *Lee*, 2013; *Tsurutani*, 1991; *Mazelle et al.*, 1997].

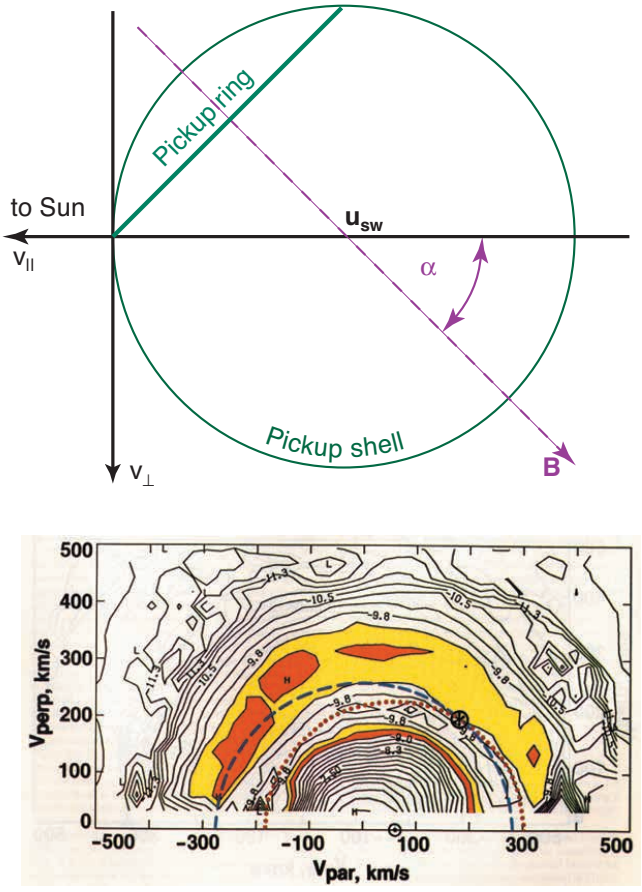

Figure 8. Illustration of the pickup velocity space distribution (top panel) and observed velocity space distribution at comet Halley [*Neugebauer et al.*, 1989] (bottom panel).

The combination of ambient and self-generated magnetic field turbulence pitch-angle scatters the newborn ions from the pickup ring. In a first approximation the pickup particles interact with the low frequency waves without significantly changing their energy in the average wave frame. As a result of this process the pitch angles of the pickup-ring particles are scattered on the spherical velocity space shell of radius u around the local solar wind velocity [cf. *Neugebauer et al.*, 1989]. This process is illustrated in Figure 8. The top panel shows the pickup distribution in velocity space, while the bottom panel shows Giotto observations [*Neugebauer et al.*, 1989]. In a first approximation the distribution can be represented by a velocity space shell of radius u_{sw} centered at the solar wind velocity. In this approximation each pickup particle contributes $\frac{1}{3} m_i u_{sw}^2$ to the plasma pressure.

It is interesting to note that the rate of change of the phase-space distribution function due to ion pickup (due to photoionization) can be well approximated by

$$\frac{\delta F}{\delta t} = \frac{I_0}{d_h^2} \frac{n_0}{4\pi\, \tau_i\, v^2}\, \delta\left(u_{sw} + v\right) \qquad (31)$$

where τ_i is the ionization timescale and v is the speed of the particles. We note that all odd moments of the pickup distribution function vanish, therefore the pickup population can be *exactly* described by the equations of ideal MHD (since the heat flux is identically zero and therefore the set of moment equations naturally closes with the pressure equation). This is a simple counterexample to the popular (but incorrect) statement that ideal MHD implicitly assumes Maxwellian (therefore equilibrium) velocity distribution. It does not. The correct statement is that any distribution function with identically zero heat flux terms satisfy the equations of ideal MHD.

Implanted ions were detected at comets Giacobini-Zinner, Halley, Grigg-Skjellerup and Borelli as large fluxes of energetic particles [*Coates et al.*, 1993; *Hynds et al.*, 1986; *McKenna-Lawlor et al.*, 1986; *Somogyi et al.*, 1986; *Young et al.*, 2004]. A significant part of the detected energetic ion population was observed at energies considerably larger than the pickup energy, indicating the presence of some kind of acceleration process acting on implanted ions. The primary acceleration mechanism turned out to be slow velocity diffusion of lower energy implanted ions [*Coates et al.*, 1989; *Neugebauer et al.*, 1989; *Gombosi et al.*, 1991].

4. MATHEMATICAL DESCRIPTION

There are three approaches to simulate cometary magnetospheres: magnetohydrodynamics (including extended MHD) and hybrid descriptions. Hybrid simulations consider fluid electrons and kinetic ions and they solve the standard set of kinetic equations [cf. *Szegő et al.*, 2000; *Bagdonat and Motschmann*, 2002; *Lipatov et al.*, 2002; *Katoh et al.*, 2003; *Bagdonat et al.*, 2004; *Delamere*, 2006; *Hansen et al.*, 2007; *Gortsas et al.*, 2009, 2010; *Wiehle et al.*, 2011]. Magnetofluid simulations, on the other hand, incorporate quite a bit of cometary physics into the governing equations. In this section we briefly summarize the governing multi-fluid extended MHD (XMHD) equations that describe the mass loaded cometary atmosphere. We will also briefly describe the appropriate source terms, but for details we refer the reader to the detailed paper of *Rubin et al.* [2014].

The multi-fluid XMHD equations for ionic species 's' can be written in the following form:

$$\frac{\partial \rho_s}{\partial t} + \nabla \cdot (\rho_s \mathbf{u}_s) = \frac{\delta \rho_s}{\delta t} \tag{32}$$

$$\rho_s \frac{\partial \mathbf{u}_s}{\partial t} + \rho_s (\mathbf{u}_s \cdot \nabla) \mathbf{u}_s + \nabla \cdot P_s - \rho_s \mathbf{g} - \rho_s \frac{q_s}{m_s} [\mathbf{E} + \mathbf{u}_s \times \mathbf{B}] = \rho_s \frac{\delta \mathbf{u}_s}{\delta t} \tag{33}$$

$$\frac{\partial P_s}{\partial t} + (\mathbf{u}_s \cdot \nabla) P_s + P_s (\nabla \cdot \mathbf{u}_s) + (P_s \cdot \nabla) \mathbf{u}_s + P_s \cdot (\nabla \mathbf{u}_s)^{\mathrm{T}} - \frac{q_s}{m_s} \left[P_s \times \mathbf{B} + (P_s \times \mathbf{B})^{\mathrm{T}}\right] + \nabla \cdot Q_s = \frac{\delta P_s}{\delta t} \tag{34}$$

where ρ, $\mathbf{u}$, P and Q represent mass density, bulk velocity, pressure tensor and heat flow tensor, respectively. The electric and magnetic field vectors are denoted by $\mathbf{E}$ and $\mathbf{B}$, while q is the particle charge and m is the particle mass. The $\rho_s \mathbf{g}$ term in the momentum equation represents the gravity force which can often be neglected in the case of a small object such as a comet. In addition, $\frac{\delta \rho}{\delta t}$ is the mass source rate (due to ionization, recombination and charge exchange), $\frac{\delta \mathbf{u}}{\delta t}$ is the time rate of change of the bulk velocity, and $\frac{\delta P_s}{\delta t}$ is the rate of change of the pressure tensor.

We consider the scenario when the pressure tensor is gyrotropic (all off-diagonal terms are zero) but anisotropic (the pressure can be different in the direction of the magnetic field and perpendicular to it) and the heat flow tensor describes the magnetic field aligned flow of parallel and perpendicular random energies. In this case the P and Q tensors can be written in the following form:

$$P_{ij} = p_\perp \delta_{ij} + (p_\parallel - p_\perp) b_i b_j \tag{35}$$

$$Q_{ijk} = h_\perp (\delta_{ij} b_k + \delta_{ik} b_j + \delta_{jk} b_i) + (h_\parallel - 3h_\perp) b_i b_j b_k \tag{36}$$

where $\mathbf{b}$ is the unit vector along the magnetic field, $p_\parallel$ and $p_\perp$ are the parallel and perpendicular pressure components, while $h_\parallel$ and $h_\perp$ and the field aligned flows of parallel and perpendicular random energies. We note that the scalar pressure and isotropic heat flux can be easily expressed with the help of $p_\parallel$, $p_\perp$, $h_\parallel$ and $h_\perp$:

$$p = \frac{1}{3} P_{ii} = \frac{1}{3} (p_\parallel + 2p_\perp) \tag{37}$$

$$\mathbf{h} = \frac{1}{2} Q_{ijj} = \frac{1}{2} (h_\parallel + 2h_\perp) \mathbf{b} \tag{38}$$

With these definitions of the pressure and heat flow tensors the ion momentum and pressure equations become

$$\rho_s \frac{\partial \mathbf{u}_s}{\partial t} + \rho_s (\mathbf{u}_s \cdot \nabla) \mathbf{u}_s + \nabla p_{s_\perp} - \rho_s \frac{q_s}{m_s} [\mathbf{E} + \mathbf{u}_s \times \mathbf{B}] = -\mathbf{B} \nabla_\parallel \left(\frac{p_{s_\parallel} - p_{s_\perp}}{B} \right) - \left(p_{s_\parallel} - p_{s_\perp} \right) \nabla_\parallel \mathbf{b} + \rho_s \mathbf{g} + \rho_s \frac{\delta \mathbf{u}_s}{\delta t} \tag{39}$$

$$\frac{\partial p_{s_\parallel}}{\partial t} + (\mathbf{u}_s \cdot \nabla) p_{s_\parallel} + p_{s_\parallel} (\nabla \cdot \mathbf{u}_s) + 2 p_{s_\parallel} \mathbf{b} \cdot \nabla_\parallel \mathbf{u}_s + \nabla_\parallel h_{s_\parallel} = \frac{h_{s_\parallel} - 3h_{s_\perp}}{B} \nabla_\parallel B + \frac{\delta p_{s_\parallel}}{\delta t} \tag{40}$$

$$\frac{\partial p_{s_\perp}}{\partial t} + (\mathbf{u}_s \cdot \nabla) p_{s_\perp} + 2 p_{s_\perp} (\nabla \cdot \mathbf{u}_s) - p_{s_\perp} \mathbf{b} \cdot \nabla_\parallel \mathbf{u}_s + \nabla_\parallel h_{s_\perp} = \frac{5h_{s_\perp}}{2B} \nabla_\parallel B + \frac{\delta p_{s_\perp}}{\delta t} \tag{41}$$

Equations (32), (39), (40) and (41) represent the fluid equations for each ion species. The electron continuity equation is replaced by the condition of quasi-neutrality:

$$n_e = \sum_{s=ions} Z_s n_s \tag{42}$$

where Z_s is the charge state of ion species 's'. The electron velocity can be expressed in terms of the average velocity of positive ions and the Hall term:

$$\mathbf{u}_e = \mathbf{u}_+ - \frac{\mathbf{j}}{e\, n_e} \tag{43}$$

where $\mathbf{j}$ is the current density and

$$\mathbf{u}_+ = \sum_{s=ions} \frac{Z_s\, n_s}{n_e} \mathbf{u}_s \tag{44}$$

We note that in general $\mathbf{u}_+ \neq \mathbf{u}_i$, because the charge averaged velocity is different than the mass averaged one. The electron pressure equations can be written as

$$\frac{\partial p_{e_\parallel}}{\partial t} + (\mathbf{u}_e \cdot \nabla)\, p_{e_\parallel} + p_{e_\parallel} (\nabla \cdot \mathbf{u}_e) + 2p_{e_\parallel} \mathbf{b} \cdot \nabla_\parallel \mathbf{u}_e + \nabla_\parallel h_{e_\parallel} = \frac{h_{e_\parallel} - 3h_{e_\perp}}{B} \nabla_\parallel B + \frac{\delta p_{e_\parallel}}{\delta t} \quad (45)$$

$$\frac{\partial p_{e_\perp}}{\partial t} + (\mathbf{u}_e \cdot \nabla)\, p_{e_\perp} + 2p_{e_\perp} (\nabla \cdot \mathbf{u}_e) - p_{e_\perp} \mathbf{b} \cdot \nabla_\parallel \mathbf{u}_e + \nabla_\parallel h_{e_\perp} = \frac{5h_{e_\perp}}{2B} \nabla_\parallel B + \frac{\delta p_{e_\perp}}{\delta t} \quad (46)$$

The heat flow terms are still not defined. These terms are usually taken from some other approximations, like collisional or collisionless heat conduction [cf. *Gombosi and Rasmussen*, 1991; *Hollweg*, 1976].

The transport equations are supplemented with Faraday's law, Ampère's law and Ohm's law to form a closed system of differential equations:

$$\frac{\partial \mathbf{B}}{\partial t} = -\nabla \times \mathbf{E} \quad (47)$$

$$\mu_0 \mathbf{j} = \nabla \times \mathbf{B} \quad (48)$$

$$\mathbf{E} + \mathbf{u}_e \times \mathbf{B} = -\frac{1}{en_e} \nabla p_{e_\perp} + \eta_e \mathbf{j} - \frac{B}{en_e} \nabla_\parallel \left(\frac{p_{e_\parallel} - p_{e_\perp}}{B} \mathbf{b} \right) \quad (49)$$

The three terms on the right hand side of equation (49) describe the ambipolar electric field (due to the mass difference between electrons and ions), the dissipation due to electrical resistivity and the effect of adiabatic focusing.

The appropriate source term for comets are described in detail in a recent paper by *Rubin et al.* [2014].

5. BOW SHOCK AND COMETOSHEATH

Conservation of momentum and energy require that the solar wind be decelerated as newly born charged particles are "picked up" by the plasma flow. Continuous deceleration of the solar wind flow by mass loading is possible only up to a certain point at which the mean molecular weight of the plasma particles reaches a critical value. At this point a weak shock forms and impulsively decelerates the flow to subsonic velocities [cf. *Biermann et al.*, 1967; *Galeev et al.*, 1985; *Koenders et al.*, 2013]. Bow shock crossings were identified in the data from each of the Halley flyby spacecraft at approximately the expected locations. The shock jumps were clearly defined in many of the observations from the plasma probes and magnetometers on Giotto, VEGA and Suisei. For the other comets it is generally recognized that the pickup ions generated so much mass loading and turbulence that the shock crossing was extremely thick. The cometary "shock wave" is quite different than the "classical" planetary and interplanetary shocks, because the deceleration and dissipation is due to mass loading and wave-particle interaction which take place over a very large region with the "shock" being only the downstream boundary of an extended distributed process [cf. *Staines et al.*, 1991; *Neugebauer et al.*, 1990; *Coates et al.*, 1997; *Richter et al.*, 2011].

The cometosheath is located between the cometary shock and the magnetic field free region in the innermost coma. The plasma population in the cometosheath is a changing mixture of ambient solar wind and particles picked up upstream and downstream of the shock. The distinction between cometary particles picked up outside and inside the shock is important because of the large difference in their random energy. The random energy of ions in a pickup shell is typically 20 keV for water group ions picked up upstream of the shock. Cometary ions born behind the shock are picked up at smaller velocities, and consequently, the random energy of their pickup shell is significantly smaller than that of ions born upstream of the shock. Overall, ions retain (in their energy) a memory of where they were born, and the plasma frame energy of pickup ions decreases with decreasing cometocentric distance. The observed distribution functions are therefore quite complicated [cf. *Mukai et al.*, 1986; *Neugebauer et al.*, 1990].

One of the debated issues is whether or not energetic electrons are a permanent feature of the cometosheath. The electron spectrometer on Giotto observed large fluxes of energetic ($0.8 - 3.6$ keV) electrons in the so called "mystery region" between about 8.5×10^3 and 5.5×10^3 km [*Rème*, 1991]. At a cometocentric distance of about 5.5×10^3 km these fluxes abruptly disappeared, simultaneously with a sudden decrease of the total ion density and velocity and an increase of the ion temperature. At the same time the magnetic field changed direction and became much smoother. *Rème* [1991] interpreted this change as a permanent feature of the cometosheath and found similar events in the Vega and Suisei data sets. A different view was presented by *Gringauz and Verigin* [1991], who did not see evidence of the presence of energetic electrons in the cometosheath and interpret the Giotto energetic electron event as a transient feature generated by a passing interplanetary disturbance.

Another very interesting feature in the cometosheath is the *cometopause*, discovered by the Vega plasma instrument [*Gringauz et al.*, 1986].

At around 1.65×10^5 km the PLASMAG instrument observed a sharp transition from a primarily solar wind proton dominated plasma population to a mainly cometary water group ion plasma. This transition was also accompanied by a moderate increase in the low frequency plasma wave intensity, while there were no obvious changes in the magnetic field. The unexpected feature of the cometopause was not its existence, but its sharpness. *Gombosi* [1987] suggested that an "avalanche" of charge exchange collisions in the decelerating plasma flow can rapidly deplete the solar wind proton population and replace it with slower water group ions.

6. COMETARY MAGNETOTAILS

Cometary magnetotails are formed by the draping of the interplanetary magnetic field (IMF) around the diamagnetic cavity boundary [*Alfvén*, 1957]. Cometary ions that are ionized outside the diamagnetic cavity get embedded into the decelerated solar wind plasma and move downstream into the tail. As the contaminated plasma flow moves downtail it is gradually accelerated to the ambient solar wind speed while the draped magnetic field lines return to their original configuration. Near the center of the tail the two magnetic lobes are separated by a current sheet and the embedded cometary ions are concentrated near this neutral sheet. These cometary ions can be observed through resonance fluorescence processes [cf. *Feldman et al.*, 2005; *Lisse et al.*, 2005; *Ip*, 2005]. A nice summary of cometary magnetotail observations can be found in *Jones et al.* [2010].

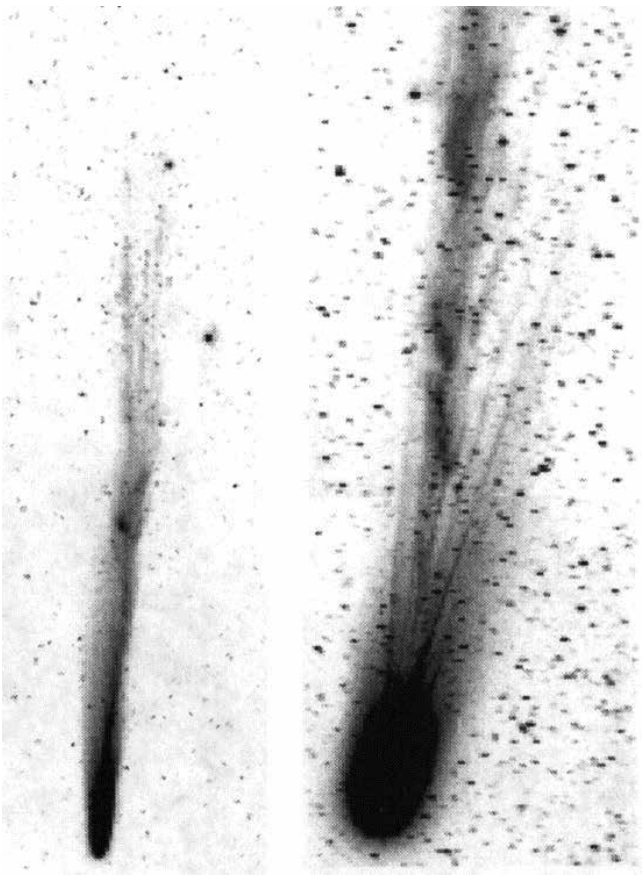

Figure 9. Dynamical structures in the long tail of comet Kohoutek. Narrow beams/jets, Kelvin-Helmholtz waves and disconnection events can be seen. (from *Lundin and Barabash* [2004])

Since cometary magnetotails are essentially draped interplanetary magnetic field lines they are very sensitive to changes in the solar wind. When a plasma tail interacts with dynamical structures in the solar wind (such as sector boundaries, corotating interaction regions, interplanetary shocks, coronal mass ejections and other transient phenomena) the tail itself can get distorted or even disconnected from the comet [cf. *Brandt et al.*, 1999]. Figure 9 shows two images of the tail of comet Kohoutek [*Lundin and Barabash*, 2004]) revealing narrow jets (or beams), wavy (Kelvin-Helmholtz unstable) structures and disconnection events.

Jia et al. [2009] simulated the tail disconnection event on April 20, 2007 on comet 2P/Encke, caused by a coronal mass ejection (CME) at a heliocentric distance of 0.34 AU. The MHD simulation reproduced the interaction process and demonstrated how the CME triggered a tail disconnection.The CME disturbed the comet with a combination of a 180° sudden rotation of the IMF, followed by a 90° gradual rotation. The simulation results are shown in Figure 10.

At 16:10 UT, the front of the flux rope (marked by the dashed vertical white lines) is at -10^5 km, in front of the comet bow shock. The IMF is in the x-z plane so the tail appears thinner in this plane, and wider in the x-y plane. At 16:30 UT, marked by the white dashed lines, the interface of reversed field lines has formed a cone centering at the comet head. In the x-y plane, the axial component in the flux rope starts to increase behind the front, as marked by the black field lines on the left of the white dashed line. The field on the right of the white line is the old IMF pointing northward. The comet tail appears stretched in both slices. At 17:40 UT, the tip of the interface between the reversed field lines has propagated to 400,000 km. Magnetic reconnection in the tail has generated a density pileup region, which appear as the trailing head of the disconnected tail. On the left of the density pileup, a new tail starts to grow. This new tail becomes wider in the x-z plane and thinner in the x-y plane, as a consequence of field rotation in the IMF. The field on the left of the white lines has both y and z components. The old field lines pointing northward are confined in the tail on the right of the white lines. At 18:30 UT, the axis of the flux

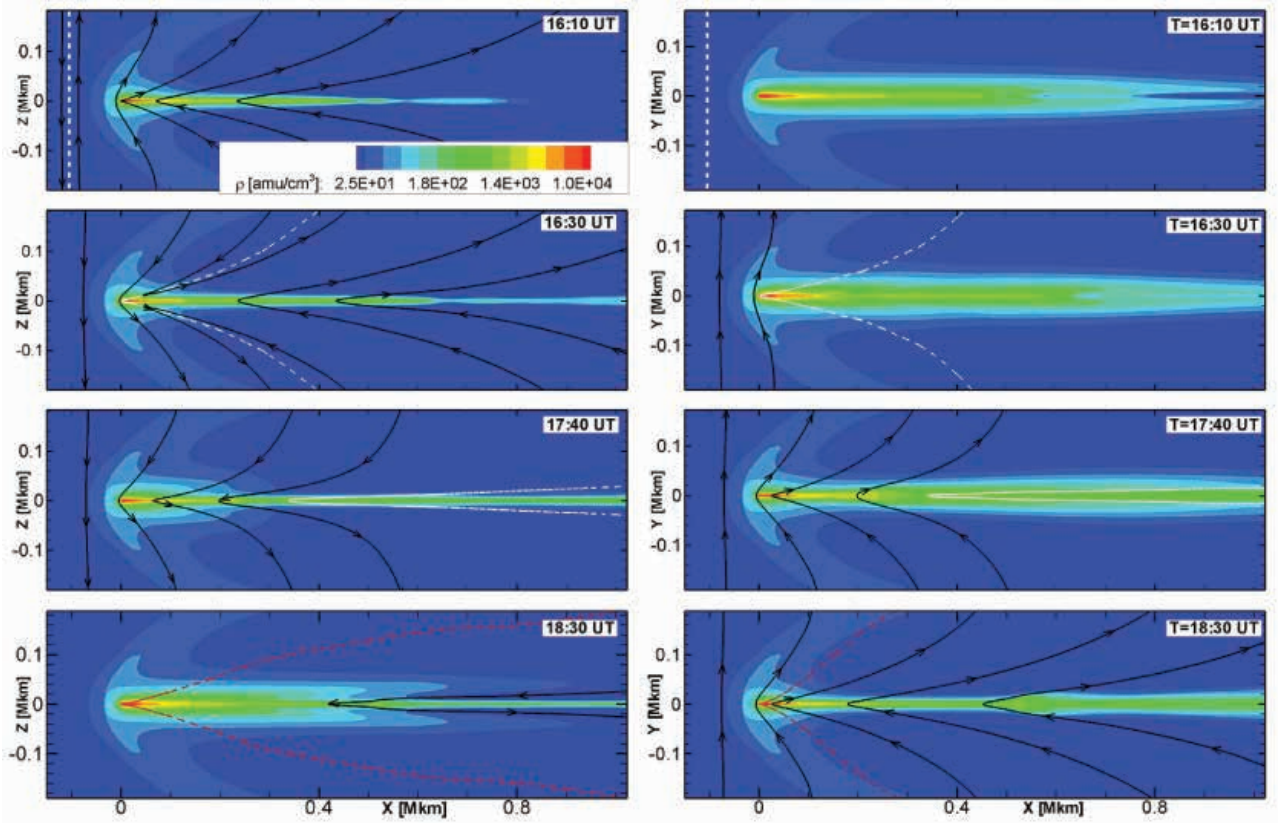

Figure 10. Time evolution of the disconnection event in two-dimensional slices. Color contours represent plasma density showing the bow shock and tail. The black lines represent magnetic field lines. White dotted lines show the current sheets, while red dashed lines show the location of the flux rope axis. Left panels show the meridional plane, while panels on the right show the ecliptic plane. (from *Jia et al.* [2009])

rope is significantly bent, as marked by the red dotted line in the left panel. At the top boundary, the axis of the flux rope has passed through the shown region. Along the x-axis, the center of the flux rope has only propagated to the inner coma, while the front of the flux rope has also passed through the shown region. The IMF along this red line is primarily in the y-direction (z-axis component), while those on the right of the red line are rotating from the y-direction to the z-direction as they leave the red line. The red line in the right panel marks the interface of the field lines with the same orientation. This stretched red line suggests that the highly draped field lines significantly affect the force balance in the interaction process, and thus control the evolution speed of this process.

The first *in situ* measurements of cometary magnetotails was carried out by the International Cometary Explorer (ICE) mission, that crossed the tail of comet Giacobini-Zinner at a distance of about 8,000 km [*Bame et al.*, 1986; *Hynds et al.*, 1986; *Ipavich et al.*, 1986; *Ogilvie et al.*, 1986; *Scarf et al.*, 1986; *Smith et al.*, 1986]. ICE started its life as the third International Sun-Earth Explorer (ICEE-3) in 1978. In the early 1980s it was recognized that using the available fuel and five gravitational encounters with the Moon the spacecraft could intercept comet Giacobini-Zinner. Since ICE was originally designed as space physics mission it did not carry any cameras, but it was well instrumented to study the plasma environment of the comet. The lack of remote sensing instruments

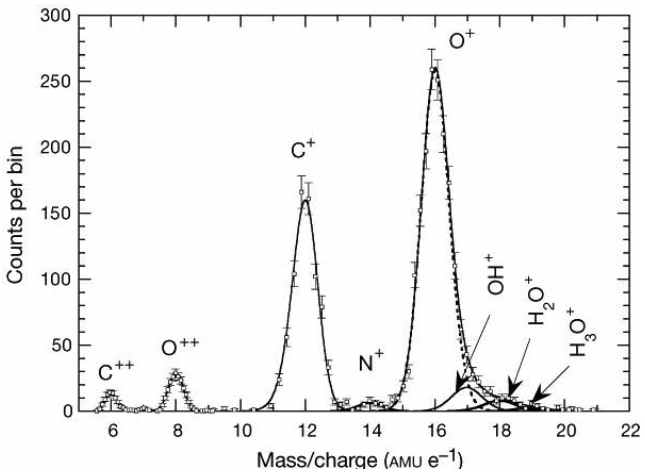

Figure 11. Mass per charge spectrum obtained during the crossing of the distant tail of comet Hyakutake. Resolved ion species include (from left to right) C^{++}, N^{++}, O^{++}, C^{+}, N^{+} and O^{+}. (from *Gloeckler et al.* [2000])

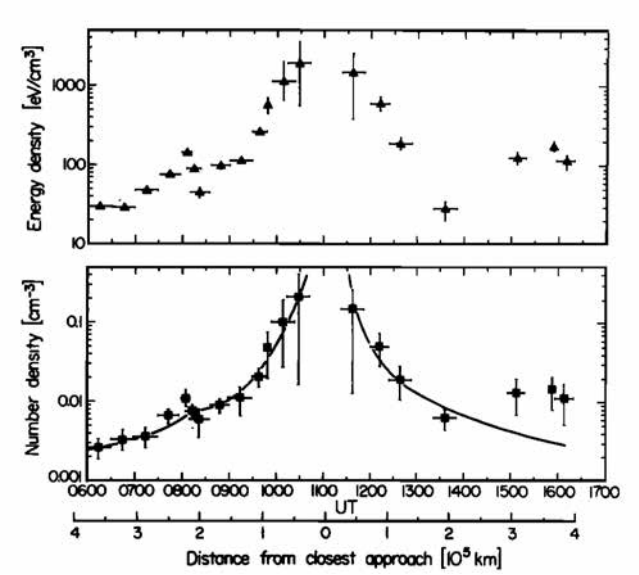

Figure 12. Variation of the energy density (upper panel) and nmnber density (lower panel) of cometary water-group pick-up ions with time and distance from closest approach from the nucleus of Giacobini-Zinner. (from *Gloeckler et al.* [1986])

made it possible to fly ICE through the comet tail, since there was no possibility to observe the illuminated side of the comet.

During the encounter the ICE spacecraft observed very high levels of hydromagnetic turbulence generated by the ion pickup process [*Scarf et al.*, 1986] and a large increase in water-group ion density [*Hynds et al.*, 1986; *Ipavich et al.*, 1986; *Ogilvie et al.*, 1986]. Figure 12 shows that the water-group number density increased by two orders of magnitude as the spacecraft reached closest approach [*Gloeckler et al.*, 1986].

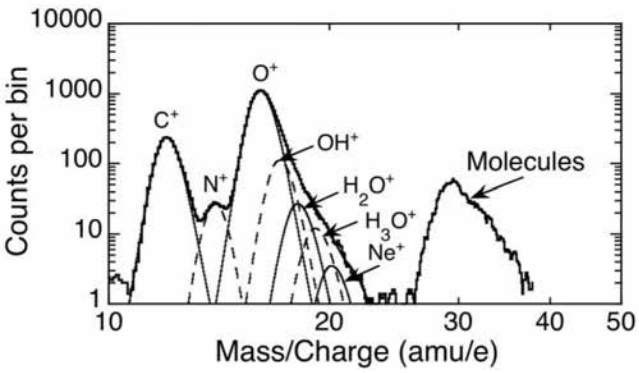

Figure 13. Mass per charge spectrum obtained during the crossing of the distant tail of comet McNaught. (from *Neugebauer et al.* [2007])

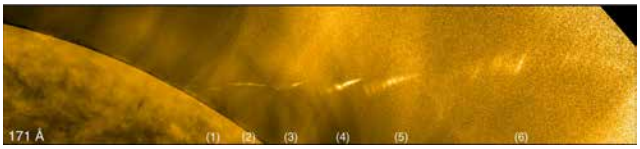

Figure 14. 171 ÅAIA images of the tail of comet Lovejoy after perihelion. The images were taken at six times: (1) 00:41:36 UT (2) 00:43:00 (3) 00:44:12 (4) 00:46:12 (5) 00:48:12 (6) 00:56:00. One can see the dramatic changes in the tail of the comet. (from *McCauley et al.* [2013])

The Ulysses spacecraft had two distant unplanned comet tail crossings. On May 1, 1996 it crossed the tail of comet Hyakutake at a distance of $\sim 5 \times 10^8$ km (3.73 AU). The Solar Wind Ion Composition Spectrometer (SWICS) identified a number of species that are most likely of cometary origin [*Gloeckler et al.*, 2000]. Figure 11 shows the mass per charge spectrum of these ions. We note the dominance of water group ions (O^+, OH^+, H_2O^+ and H_3O^+). Particularly telling is the presence of H_3O^+ that is collisionally created in water vapor dominated regions by the $H_2O + H_2O^+ \rightarrow H_3O^+ + OH$ reaction.

Ulysses had a second unplanned comet tail crossing in February 2007, when it crossed the ion tail of comet McNaught [*Neugebauer et al.*, 2007]. Inspection of Figure 13 reveals that the mass per charge spectrum of heavy ions was quite similar to the one observed during the Hyakutake tail crossing, confirming the dominance of water group ions.

Recent interest focuses on the tail dynamics of sungrazing comets. The most significant sungrazer since the launch of the Solar Dynamics Observatory (SDO) is comet Lovejoy. Detailed, high resolution observations of the perihelion passage of this comet were carried out by the SDO/AIA instrument [*McCauley et al.*, 2013].

Comet Lovejoy reached perihelion on December 16, 2011 as it passed approximately 140,000 km above the photosphere. Since the comet survived perihelion, it is thought that the size of the nucleus must have been about 500 m. During the coronal passage, it is believed that a significant fraction of the comet's mass was burned off.

It was a surprise that comet Lovejoy survived perihelion. Figure 14 shows a series of images taken after it passed 0.2 $R_\odot$ above the photosphere. The series of photographs show that the tail becomes unstable and it eventually detaches from the nucleus. Sungrazing comets are becoming important not only because they provide new insights into the physics of comets, but also because they help us to understand the thermal structure of the low solar corona. In effect, these comets provide a tool to probe regions that are not accessible to *in situ* observations.

Simulating the interaction of sungrzaing comets with the low solar corona is very challenging, because one needs to carry out a realistic low corona simulation before the rapidly moving comet (typical speeds are $\sim$ 500 km/s) can be inserted into this background. The first attempts for such sim-

ulations are just being made [*Downs et al.*, 2013], but significant additional progress is required before we can carry out more realistic simulations.

7. MODEL-DATA COMPARISON

Until the arrival of the Rosetta spacecraft to comet Churyumov-Gerasimenko [*Glassmeier et al.*, 2007] comet Halley remains the best studied active comet, using observational, theoretical and simulation methods. The Giotto spacecraft flew within $\sim$ 600 kilometers of the nucleus and it provided a wealth of data not only about the global plasma environment (density, velocity, temperature and magnetic field) but also about the composition of the ionized and neutral gases. Recently *Rubin et al.* [2014] carried out a detailed comparison between a multifluid MHD simulation and Giotto observation. In this section we review the highlights of this study.

The simulation of *Rubin et al.* [2014] solves separate equations for solar wind protons, cometary light and heavy ions and electrons. The cometary light ions are mainly H^+, but they are separately treated from the solar wind. The cometary heavy ions are dominated by water group ions, with relatively small contribution from carbon and nitrogen bearing molecules and other species. Mass loading, charge-exchange, dissociative ion-electron recombination, and collisional interactions between the fluids are taken into account. The computational domain spans over several million kilometers and the close vicinity of the comet is resolved to the details of the magnetic cavity. Simulation results are compared with the data of the JPA [*Johnstone et al.*, 1986] and IMS [*Balsiger et al.*, 1986] instruments.

Figure 15 shows the comparison of the simulated and measured ion mass densities along the Giotto trajectory. The solid lines show the model results while the measurements from the JPA instrument [*Formisano et al.*, 1990] and the IMS [*Altwegg et al.*, 1993] are denoted by the dots. The

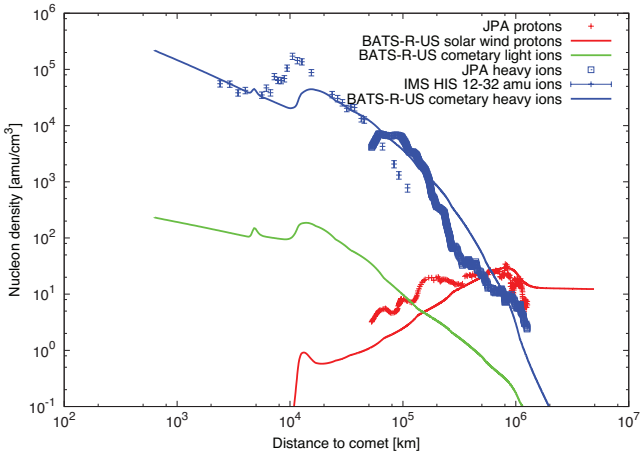

Figure 15. Nucleon density (in units of amu/cm^3) along Giotto's inbound trajectory. The x-axis denotes the distance to the comet [km] with the closest approach at roughly 600 km. The solid lines show the simulated densities of the solar wind protons, the cometary light ions, and the cometary heavy ions. The corresponding measurements are added, i.e. the observations of the heavy ions by the JPA [*Formisano et al.*, 1990] and the IMS [*Altwegg et al.*, 1993] instruments. (from *Rubin et al.* [2014])

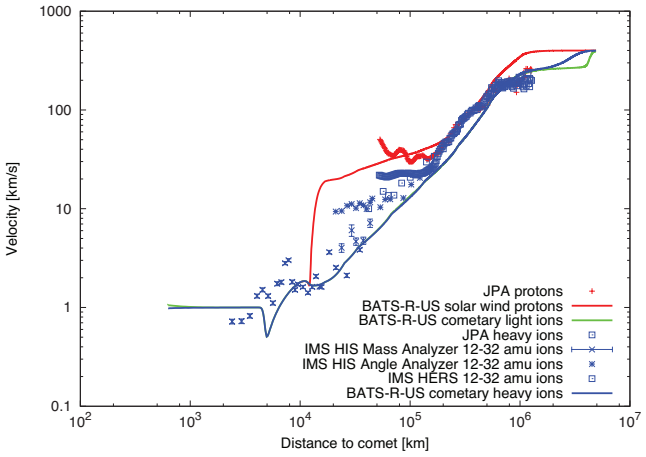

Figure 16. Ion velocities [km/s] along Giottos inbound trajectory. The x-axis denotes the distance to the comet [km] with the closest approach at roughly 600 km. The solid lines show the modeled bulk speeds of the solar wind protons, the cometary light ions, and the cometary heavy ions. The corresponding measurements are added, i.e. the heavy ion velocity by the JPA [*Formisano et al.*, 1990] and the IMS [*Altwegg et al.*, 1993] instruments. (from *Rubin et al.* [2014])

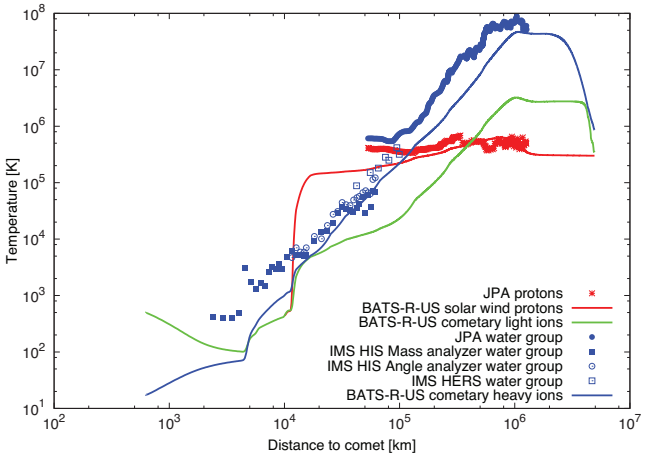

Figure 17. Ion temperatures [K] along Giottos inbound path. The x-axis denotes the distance to the comet [km]. The solid lines show the modeled temperatures of the solar wind protons, the cometary light ions, and the cometary heavy ions. The corresponding measurements are also given: the observations of the protons and the heavy ions by the JPA [*Formisano et al.*, 1990] and the IMS [*Altwegg et al.*, 1993] instruments. (from *Rubin et al.* [2014])

lack of solar wind protons in the vicinity of the comet becomes clearly visible inside approximately 100,000 km from the comet along the Giotto trajectory. The proton population originating from the Sun is deflected around the cavity and also slowed down due to the abundant elastic collisions with the neutral coma which leads to an enhancement in density before it is then lost due to the charge-exchange with the neutral gas as discussed earlier. This leads to a slight enhancement at roughly 10,000 km which is not symmetric around the cavity.

The model reproduces the ion pile-up for both the cometary light and heavy plasma species at around 10,000 to 20,000 kilometers from the nucleus although less prominently than measured. Generally, the model indicates that the pile-up region of the light cometary ions and the heavy ones do not have to be exactly co-located given the slightly different temperature dependence of ion-electron recombination rates and the more extended gas distribution of the cometary daughter species. Closer to the nucleus the model shows the formation of the inner shock. Also the radial distribution of the water group ions is steeper than for the cometary light ions, again the result of the faster decrease of the abundance of the cometary parent species with distance from the nucleus.

Figure 16 shows the simulated ion bulk velocities compared to the measurements [*Formisano et al.*, 1990; *Altwegg et al.*, 1993]. Close to the comet (inside ∼10,000 km from the nucleus) the velocity vectors and bulk speeds of the cometary ions are tightly coupled through ion – ion, ion – neutral, and ion – electron interactions while the solar wind protons are already attenuated in this region.

In Figure 17 the simulated temperatures of the individual ion species are compared to those derived from the IMS and JPA instruments. It can be seen that the temperature difference between the solar wind and the pick-up populations is quite well reproduced by the MHD model.

Overall, the agreement between observations and the detailed simulation results of *Rubin et al.* [2014] is quite remarkable.

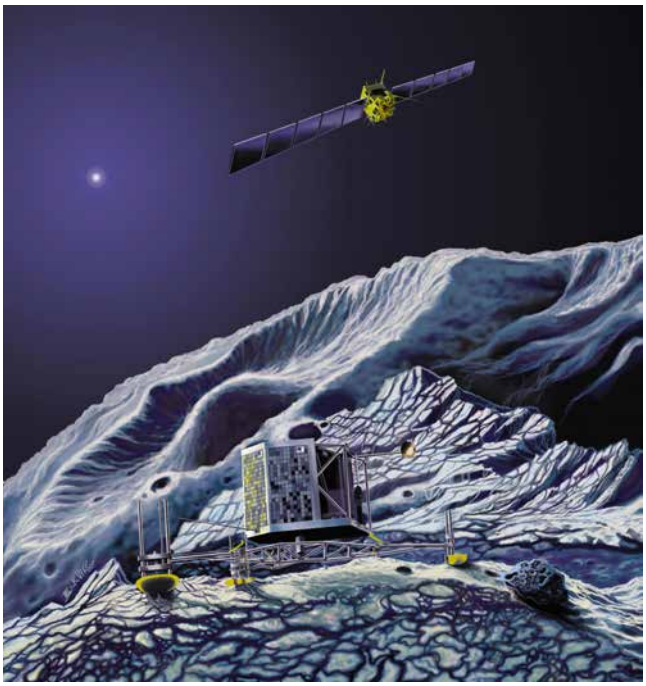

Figure 18. Artist's illustration of the Rosetta orbiter comet with lander on the surface of comet Churyumov-Gerasimenko (courtesy of NASA JPL).

8. ROSETTA

The goal of this paper was to summarize our pre-Rosetta mission understanding of cometary magnetospheres. This understanding is based on ground-based observations and a small number of short duration flyby missions. It is highly likely that some of the ideas we outlined in this paper will be modified or even rejected after we gain a detailed, long-duration insight into the way comet Churyumov-Gerasimenko behaves as it becomes active, approaches its perihelion and then gradually fades.

In early 2014 Rosetta will wave up from hibernation will start preparations for its comet encounter. In November 2014 it will deliver a lander unit, called PHILAE. After the lander delivery the Rosetta orbiter will start its 13 months long "escort" phase. During the prime mission Churyumov-Gerasimenko will pass through perihelion in August 2015. The spacecraft is well instrumented for both *in-situ* and remote sensing observations [cf. *Glassmeier et al.*, 2007]. Figure 18 shows an artist's illustration of the Rosetta orbiter and PHILAE lander at comet Churyumov-Gerasimenko

Rosetta's target comet is moderately active near perihelion. *Snodgrass, C. et al.* [2013] estimated comet Churyumov-Gerasimenko's pre-perihelion water production rate curve as

$$Q\,(\mathrm{H_2O}) = \frac{2.3 \times 10^{28}}{d_h^{5.9}} \quad \text{molecules/s} \qquad (50)$$

implying that Rosetta will encounter production rates of $Q \sim 6 \times 10^{24}$ molecules/s at $d_h = 4$ AU, $\sim 3 \times 10^{25}$ at 3 AU, and 4×10^{26} at 2 AU. At perihelion ($d_h = 1.3$ AU) one can expect a water production rate of 5×10^{27} molecules/s. This value is about two orders of magnitude smaller than the production rate of comet Halley was during the Giotto encounter.

The expectation is that the nucleus will be practically inactive during the initial phase of the

Rosetta mission when the heliocentric distance will be around $d_h \approx 2.5$ AU. This is the phase when the lander can carry out its main mission, the *in situ* examination of the nucleus. As the comet approaches the Sun it will start to develop higher and higher activity levels. During this phase the cometary magnetosphere will gradually develop. Initially the magnetosphere will be fully kinetic, due to the very low density of the cometary neutral ionosphere and ionosphere

ACKNOWLEDGMENTS. This work has been supported by the US Rosetta Project (JPL subcontract 1266313 under NASA grant NMO710889) and by NSF grant AST-0707283. Valuable discussions with Drs. Michael Combi, Ying-Dong Jia and Martin Rubin are gratefully acknowledged. The author would also like to thank two referees for their valuable comments that helped to improve the original manuscript.

REFERENCES

Alfvén, H. (1957), On the theory of comet tails, *Tellus*, *9*, 92–96.

Altwegg, K., H. Balsiger, J. Geiss, R. Goldstein, W. Ip, A. Meier, M. Neugebauer, H. Rosenbauer, and E. Shelley (1993), The ion population between 1300 km and 230 000 km in the coma of comet P/Halley, *Astron. Astrophys.*, *279*, 260–266.

Bagdonat, T., and U. Motschmann (2002), From a weak to a strong comet - 3D global hybrid simulation studies, *Earth Moon and Planets*, *90*, 305–321, doi:{10.1023/A:1021578232282}.

Bagdonat, T., U. Motschmann, K. Glassmeier, and E. Khurt (2004), Plasma environment of Comet Churyumov-Gerasimenko 3D hybrid code simulations, in *New Rosetta Targets: Observations, Simulations and Instrument Performances*, *Astrophysics and Space Science Library*, vol. 311, edited by Colangeli, L and Epifani, EM and Palumbo, P, pp. 153–166, Giunta Reg Della Campania; Osservator Astronom Capodimonte; Univ Degli Studi Napoli.

Balsiger, H., K. Altwegg, F. Bühler, J. Geiss, A. G. Ghielmetti, B. E. Goldstein, R. Goldstein, W. T. Huntress, W.-H. Ip, A. J. Lazarus, A. Meier, M. Neugebauer, U. Rettenmund, H. Rosenbauer, R. Schwenn, R. D. Sharp, E. G. Shelley, E. Ungstrup, and D. T. Young (1986), Ion composition and dynamics at comet Halley, *Nature*, *321*, 330–334.

Bame, S. J., R. C. Anderson, J. R. Asbridge, D. N. Baker, W. C. Feldman, S. A. Fuselier, J. T. Gosling, D. J. Mccomas, M. F. Thomsen, D. T. Young, and R. D. Zwickl (1986), Comet Giacobini-Zinner: Plasma description, *Science*, *232*, 356–361, doi:10.1126/science.232.4748.356.

Banks, P. M., and G. Kockarts (1973), *Aeronomy*, Academic Press, New York.

Benna, M., and P. Mahaffy (2007), Multi-fluid model of comet 1P/Halley, *Planet. Space Sci.*, *55*, 1031 – 1043, doi:10.1016/j.pss.2006.11.019.

Biermann, L. (1951), Kometenschweife und Solare Korpuskularstrahlung, *Zeitschrift für Astrophysik*, *29*, 274–286.

Biermann, L., B. Brosowski, and H. U. Schmidt (1967), The interaction of the solar wind with a comet, *Sol. Phys.*, *1*, 254–284.

Brandt, J. C., F. M. Caputo, J. T. Hoeksema, M. B. Niedner, Y. Yi, and M. Snow (1999), Disconnection events (DEs) in Halley's comet 19851986:: The correlation with crossings of the heliospheric current sheet (HCS), *Icarus*, *137*, 69–83, doi:10.1006/icar.1998.6030.

Coates, A., and G. Jones (2009), Plasma environment of jupiter family comets, *Planet. Space Sci.*, *57*, 1175 – 1191, doi:http://dx.doi.org/10.1016/j.pss.2009.04.009.

Coates, A., A. Johnstone, B. Wilken, K. Jockers, and K. Glassmeier (1989), Velocity space diffusion of pickup ions from the water group at comet Halley, *J. Geophys. Res.*, *94*, 9983–9993, doi:10.1029/JA094iA08p09983.

Coates, A. J., A. D. Johnstone, B. Wilken, and F. Neubauer (1993), Velocity space diffusion and nongyrotropy of pickup water group ions at comet Grigg-Skjellerup, *J. Geophys. Res.*, *98*, 20,985, doi:10.1029/93JA02535.

Coates, A. J., C. Mazelle, and F. M. Neubauer (1997), Bow shock analysis at comets Halley and Grigg-Skjellerup, *J. Geophys. Res.*, *102*, 7105–7113, doi:10.1029/96JA04002.

Combi, M. R., V. M. Tenishev, M. Rubin, N. Fougere, and T. I. Gombosi (2012), Narrow dust jets in a diffuse gas coma: A natural product of small active regions on comets, *Astrophys. J.*, *749*(1), 29, doi:10.1088/0004-637X/749/1/29.

Cravens, T. E. (1986), The physics of the cometary contact surface, in *Proc. 20th ESLAB Symposiumo on the Exploration of Halley's Comet*, vol. ESA SP-250, pp. 241–246, Eur. Space Agency.

Cravens, T. E. (1989), A magnetohydrodynamical model of the inner coma of comet Halley, *J. Geophys. Res.*, *94*, 15,025–15,040, doi:10.1029/JA094iA11p15025.

Cravens, T. E., and A. Körösmezey (1986), Vibrational and rotational cooling of electrons by water-vapor, *Planet. Space Sci.*, *34*, 961–970, doi:10.1016/0032-0633(86)90005-X.

Cravens, T. E., N. Ozak, M. S. Richard, M. E. Campbell, I. P. Robertson, M. Perry, and A. M. Rymer (2011), Electron energetics in the Enceladus torus, *J. Geophys. Res.*, *116*, n/a–n/a, doi:10.1029/2011JA016498.

Davidsson, B. J. R. (2008), Comet Knudsen layers, *Space Sci. Rev.*, *138*, 207–223, doi:10.1007/s11214-008-9305-8.

Delamere, P. A. (2006), Hybrid code simulations of the solar wind interaction with Comet 19P/Borrelly, *J. Geophys. Res.*, *111*, doi:{10.1029/2006JA011859}.

Delsemme, A., and D. Miller (1971), Physico-Chemical Phenomena in Comets, III. Continuum of Comet Burnham (1960 II), *Planet. Space Sci.*, *19*, 1229–1257, doi:10.1016/0032-0633(71)90180-2.

Delsemme, A. H., and P. Swings (1952), Hydrates de gaz dans les noyaux cométaires et les grains interstellaires, *Ann. Astrophys.*, *15*, 1.

Downs, C., J. A. Linker, Z. Mikič, P. Riley, C. J. Schrijver, and P. Saint-Hilaire (2013), Probing the solar magnetic field with a sun-grazing comet, *Science*, *340*(6137), 1196–1199, doi:10.1126/science.1236550.

Feldman, P. D., A. L. Cochran, and M. R. Combi (2005), Spectroscopic investigations of fragment species in the coma, in *Comets II*, edited by M. C. Festou, U. Keller, and H. A. Weaver, pp. 425–447, University of Arizona Press.

Formisano, V., E. Amata, M. B. Cattaneo, P. Torrente, A. Johnstone, A. Coates, and B. Wilken (1990), Plasma-flow inside comet P/Halley, *Astron. Astrophys.*, *238*, 401–412.

Fougere, N., M. Combi, M. Rubin, and V. Tenishev (2013), Modeling the heterogeneous ice and gas coma of comet 103P/Hartley 2, *Icarus*, *225*, 688 – 702, doi:10.1016/j.icarus.2013.04.031.

Galeev, A. A., T. E. Cravens, and T. I. Gombosi (1985), Solar wind stagnation near comets, *Astrophys. J.*, *289*, 807–819.

Gan, L., and T. E. Cravens (1990), Electron energetics in the inner coma of comet halley, *J. Geophys. Res.*, *95*, 6285–6303, doi:10.1029/JA095iA05p06285.

Glassmeier, K.-H., H. Boehnhardt, D. Koschny, E. Kührt, and I. Richter (2007), The Rosetta mission: Flying towards the origin of the solar system, *Space Sci. Rev.*, *128*, 1–21, doi:10.1007/s11214-006-9140-8.

Gloeckler, G., D. Hovestadt, F. M. Ipavich, M. Scholer, B. Klecker, and A. B. Galvin (1986), Cometary pick-up ions observed near Giacobini-Zinner, *Geophys. Res. Lett.*, *13*, 251–254, doi:10.1029/GL013i003p00251.

Gloeckler, G., J. Geiss, N. A. Schwadron, L. A. Fisk, T. H. Zurbuchen, F. M. Ipavich, R. von Steiger, H. Balsiger, and B. Wilken (2000), Interception of comet Hyakutake's ion tail at a distance of 500 million kilometres, *Nature*, *404*, 576–578.

Goldstein, B. E., K. Altwegg, H. Balsiger, S. A. Fuselier, W.-H. Ip, A. Meier, M. Neugebauer, H. Rosenbauer, and R. Schwenn (1989), Observations of a shock and a recombination layer at the contact surface of comet Halley, *J. Geophys. Res.*, *94*, 17,251–17,257, doi:10.1029/JA094iA12p17251.

Gombosi, T. I. (1987), Charge exchange avalanche at the cometopause, *Geophys. Res. Lett.*, *14*, 1174–1177, doi:10.1029/GL014i011p01174.

Gombosi, T. I., and C. E. Rasmussen (1991), Transport of gyration dominated space plasmas of thermal origin I.: Generalized transport equations, *J. Geophys. Res.*, *96*, 7759.

Gombosi, T. I., A. F. Nagy, and T. E. Cravens (1986), Dust and neutral gas modeling of the inner atmospheres of comets, *Rev. Geophys.*, *24*(3), 667–700.

Gombosi, T. I., M. Neugebauer, A. Johnstone, A. Coates, and D. Huddleston (1991), Comparison of observed and calculated implanted ion distributions outside comet halley's bow shock, *J. Geophys. Res.*, *96*, 467.

Gombosi, T. I., D. L. De Zeeuw, R. M. Häberli, and K. G. Powell (1996), Three-dimensional multiscale MHD model of cometary plasma environments, *J. Geophys. Res.*, *101*(A7), 15,233–15,253.

Gortsas, N., U. Motschmann, E. Kuehrt, J. Knollenberg, S. Simon, and A. Boesswetter (2009), Mapping of coma anisotropies to plasma structures of weak comets: a 3-D hybrid simulation study, *Ann. Geophys.*, *27*, 1555–1572.

Gortsas, N., U. Motschmann, E. Kuehrt, K. Glassmeier, K. C. Hansen, J. Mueller, and A. Schmidt (2010), Global plasma-parameter simulation of Comet 67P/Churyumov-Gerasimenko approaching the Sun, *Astron. Astrophys.*, *520*, doi:{10.1051/0004-6361/201014761}.

Gringauz, K., T. Gombosi, A. Remizov, I. Apathy, I. Szemerey, M. I. Verigin, L. I. Denchikova, A. V. Dyachkov, E. Keppler, I. N. Klimenko, A. K. Richter, A. J. Somogyi, K. Szego, S. Szendro, M. Tatrallyay, A. Varga, and G. A. Vladimirova (1986), First in situ plasma and neutral gas measurements at comet Halley, *Nature*, *321*, 282–285, doi:10.1038/321282a0.

Gringauz, K. I., and M. I. Verigin (1991), Permanent and nonstationary plasma phenomena in comet Halley's head, in *Cometary Plasma Processes*, *AGU Geophysical Monograph Series*, vol. 61, edited by A. D. Johnstone, pp. 107–116, American Geophysical Union, Washington, D.C.

Häberli, R. M., M. R. Combi, T. I. Gombosi, D. . L. De Zeeuw, and K. G. Powell (1997), Quantitative analysis of H_2O^+ coma images using a multiscale MHD model with detailed ion chemistry, *Icarus*, *130*, 373–386.

Hansen, K. C., T. Bagdonat, U. Motschmann, C. Alexander, M. R. Combi, T. E. Cravens, T. I. Gombosi, Y. Jia, and I. P. Robertson (2007), The plasma environment of comet 67P/Churyumov-Gerasimenko throughout the Rosetta main mission, *Space Sci. Rev.*, *128*, 133–166, doi:{10.1007/s11214-006-9142-6}.

Hollweg, J. V. (1976), Collisionless electron heat conduction in the solar wind, *J. Geophys. Res.*, *81*, 1649–1658, doi:10.1029/JA081i010p01649.

Hynds, R., S. Cowley, T. Sanderson, K. Wenzel, and J. Vanrooijen (1986), Observations of energetic ions from comet Giacobini-Zinner, *Science*, *232*, 361–365, doi:10.1126/science.232.4748.361.

Ip, W. (2005), Global solar wind interaction and ionospheric dynamics, in *Comets II*, edited by M. C. Festou, U. Keller, and H. A. Weaver, pp. 605–629, University of Arizona Press.

Ip, W.-H., and W. I. Axford (1987), The formation of a magnetic-field-free cavity at comet Halley, *Nature*, *325*, 418–419, doi:10.1038/325418a0.

Ipavich, F. M., A. B. Galvin, G. Gloeckler, D. Hovestadt, B. Klecker, and M. Scholer (1986), Comet Giacobini-Zinner: In situ observations of energetic heavy ions, *Science*, *232*, 366–369, doi:10.1126/science.232.4748.366.

Jia, Y. D., C. T. Russell, L. K. Jian, W. B. Manchester, O. Cohen, A. Vourlidas, K. C. Hansen, M. R. Combi, and T. I. Gombosi (2009), Study of the 2007 April 20 CME-comet interaction event with an MHD model, *Astrophys. J. Lett.*, *696*, L56, doi:10.1088/0004-637X/696/1/L56.

Johnstone, A., A. Coates, S. Kellock, B. Wilken, K. Jockers, H. Rosenbauer, W. Studemann, W. Weiss, V. Formisano, E. Amata, R. Cerulli-Irelli, M. Dobrowolny, R. Terenzi, A. Egidi, H. Borg, B. Hultquist, J. Winningham, C. Gurgiolo, D. Bryant, T. Edwards, W. Feldman, M. Thomsen, M. K. Wallis, L. Biermann, H. Schmidt, R. Lust, G. Haerendel, and G. Paschmann (1986), Ion flow at comet Halley, *Nature*, *321*, 344–347, doi:10.1038/321344a0.

Jones, G. H., R. J. Forsyth, and A. J. Coates (2010), The structure of comets' induced magnetotails: Remote and in situ observations, in *Pickup Ions Throughout the Heliosphere and Beyond*, *AIP Conf. Proc.*, vol. 1302, edited by J. A. le Roux, V. Florinski, G. P. Zank, and A. J. Coates, pp. 225–230, American Institute of Physics, doi:10.1063/1.3529974.

Katoh, Y., H. Oya, M. Iizima, and T. Ono (2003), Numerical study on the spatial extent of interaction region surrounding comet nucleus - Ion pick-up process, *Earth Planets and Space*, *55*(11), 705–711.

Koenders, C., K.-H. Glassmeier, I. Richter, U. Motschmann, and M. Rubin (2013), Revisiting cometary bow shock positions, *Planet. Space Sci.*, p. in press, doi:http://dx.doi.org/10.1016/j.pss.2013.08.009.

Körösmezey, A., T. Cravens, T. Gombosi, A. Nagy, D. Mendis, K. Szegö, B. Gribov, R. Sagdeev, V. Shapiro, and V. Shevchenko (1987), A New Model of Cometary Ionospheres, *J. Geophys. Res.*, *92*, 7331–7340, doi:10.1029/JA092iA07p07331.

Lee, M. A. (2013), Ultra-low frequency waves at comets, in *Plasma Waves and Instabilities at Comets and in Magnetospheres*, *AGU Geophysical Monograph Series*, vol. 53, edited by B. T. Tsurutani and H. Oya, pp. 13–29, American Geophysical Union, doi:10.1029/GM053p0013.

Lipatov, A. S., U. Motschmann, and T. Bagdonat (2002), 3D hybrid simulations of the interaction of the solar wind with a weak comet, *Planet. Space Sci.*, *50*, 403–411, doi:{10.1016/S0032-0633(02)00004-1}.

Lisse, C. M., T. E. Cravens, and K. Dennerl (2005), X-ray and extreme ultraviolet emission from comets, in *Comets II*, edited by M. C. Festou, U. Keller, and H. A. Weaver, pp. 631–643, University of Arizona Press.

Lundin, R., and S. Barabash (2004), The wakes and magnetotails of mars and venus, *Adv. Space Res.*, *33*(11), 1945 – 1955, doi:10.1016/j.asr.2003.07.054.

Mazelle, C., J. Cao, G. Belmont, F. Neubauer, and A. Coates (1997), Compressive character of low frequency waves driven by newborn ions at comet Grigg-Skjellerup, *Adv. Space Res.*, *20*(2), 267 – 270, doi:10.1016/S0273-1177(97)00544-9.

McCauley, P. I., S. H. Saar, J. C. Raymond, Y.-K. Ko, and P. Saint-Hilaire (2013), Extreme-ultraviolet and X-ray observations of comet Lovejoy (C/2011 W3) in the lower corona, *Astrophys. J.*, *768*, 161, doi:10.1088/0004-637X/768/2/161.

McKenna-Lawlor, S., E. Kirsch, D. Osullivan, A. Thompson, and K. Wenzel (1986), Energetic ions in the environment of comet Halley, *Nature*, *321*, 347–349, doi:10.1038/321347a0.

Mendis, D. A., H. L. F. Houpis, and M. L. Marconi (1985), The physics of comets, *Fundamentals of Cosmic Physics*, *10*, 1.

Mukai, T., W. Miyake, T. Terasawa, M. Kitayama, and K. Hirao (1986), Plasma observation by Suisei of solar-wind interaction with comet Halley, *Nature*, *321*, 299–303, doi:10.1038/321299a0.

Neubauer, F. M., K. H. Glassmeier, M. Pohl, J. Raeder, M. H. Acuna, L. F. Burlaga, N. F. Ness, G. Musmann, F. Mariani, M. K. Wallis, E. Ungstrup, and H. U. Schmidt (1986), First results from the giotto magnetometer experiment at comet Halley, *Nature*, *321*, 352–355, doi:10.1038/321352a0.

Neugebauer, M., A. J. Coates, and F. M. Neubauer (1990), Comparison of picked-up protons and water group ions upstream of comet Halley's bow shock, *J. Geophys. Res.*, *95*, 18,745–18,753, doi:10.1029/JA095iA11p18745.

Neugebauer, M., G. Gloeckler, J. T. Gosling, A. Rees, R. Skoug, B. E. Goldstein, T. P. Armstrong, M. R. Combi, T. Mkinen, D. J. McComas, R. von Steiger, T. H. Zurbuchen, E. J. Smith, J. Geiss, and L. J. Lanzerotti (2007), Encounter of the Ulysses spacecraft with the ion tail of comet McNaught, *Astrophys. J.*, *667*, 1262–1266, doi:10.1086/521019.

Neugebauer, M., A. Lazarus, H. Balsiger, S. Fuselier, F. Neubauer, and H. Rosenbauer (1989), The Velocity Distributions of Cometary Protons Picked up by the Solar-Wind, *J. Geophys. Res.*, *94*, 5227–5239, doi:10.1029/JA094iA05p05227.

Ogilvie, K. W., M. A. Coplan, P. Bochsler, and J. Geiss (1986), Ion composition results during the International Cometary Explorer encounter with Giacobini-Zinner, *Science*, *232*, 374–377, doi:10.1126/science.232.4748.374.

Puhl-Quinn, P., and T. E. Cravens (1995), One-dimensional hybrid simulations of the diamagnetic cavity boundary region of comet halley, *J. Geophys. Res.*, *100*, 21,631–21,644, doi:10.1029/95JA01820.

Rème, H. (1991), Cometary plasma observations between the shock and the contact surface, in *Cometary Plasma Processes*, *AGU Geophysical Monograph Series*, vol. 61, edited by A. D. Johnstone, pp. 87–105, American Geophysical Union, doi:10.1029/GM061p0087.

Richter, I., C. Koenders, K. Glassmeier, B. Tsurutani, and R. Goldstein (2011), Deep Space 1 at comet 19P/Borrelly: Magnetic field and plasma observations, *Planet. Space Sci.*, *59*, 691 – 698, doi:10.1016/j.pss.2011.02.001.

Rubin, M., K. C. Hansen, M. R. Combi, L. K. S. Daldorff, T. I. Gombosi, and V. M. Tenishev (2012), Kelvin-Helmholtz instabilities at the magnetic cavity boundary of comet 67P/Churyumov-Gerasimenko, *J. Geophys. Res.*, *117*, A06,227, doi:10.1029/2011JA017300.

Rubin, M., M. R. Combi, L. K. S. Daldorff, T. I. Gombosi, K. C. Hansen, Y. Shou, V. M. Tenishev, G. Tth, B. van der Holst, and K. Altwegg (2014), Comet 1P/Halley multifluid MHD model for the Giotto fly-by, *J. Geophys. Res.*, *119*, Axxxxx, doi:10.1029/2014JAxxxxxx.

Rubin, M., K. C. Hansen, T. I. Gombosi, M. R. Combi, K. Altwegg, and H. Balsiger (2009), Ion composition and chemistry in the coma of Comet 1P/Halley-A comparison between Giotto's Ion Mass Spectrometer and our ion-chemical network, *Icarus*, *199*(2), 505–519, doi:10.1016/j.icarus.2008.10.009.

Rubin, M., V. M. Tenishev, M. R. Combi, K. C. Hansen, T. I. Gombosi, K. Altwegg, and H. Balsiger (2011), Monte Carlo modeling of neutral gas and dust in the coma of Comet 1P/Halley, *Icarus*, *213*, 655–677, doi:10.1016/j.icarus.2011.04.006.

Sagdeev, R. Z., V. D. Shapiro, V. I. Shevchenko, and K. Szego (1986), MHD turbulence in the solar wind-comet interaction region, *Geophys. Res. Lett.*, *13*, 85–88, doi:10.1029/GL013i002p00085.

Scarf, F. L., F. V. Coroniti, C. F. Kennel, D. A. Gurnett, W. Ip, and E. J. Smith (1986), Plasma wave observations at comet Giacobini-Zinner, *Science*, *232*, 377–381, doi:10.1126/science.232.4748.377.

Schunk, R. W., and A. F. Nagy (2000), *Ionospheres – Physics, Plasma Physics, and Chemistry*, Cambridge University Press, New York.

Smith, E. J., B. T. Tsurutani, J. A. Slavin, D. E. Jones, G. L. Siscoe, and D. A. Mendis (1986), International Cometary Explorer encounter with Giacobini-Zinner: Magnetic field observations, *Science*, *232*, 382–385, doi:10.1126/science.232.4748.382.

Snodgrass, C., Tubiana, C., Bramich, D. M., Meech, K., Boehnhardt, H., and Barrera, L. (2013), Beginning of activity in 67P/Churyumov-Gerasimenko and predictions for 2014-2015, *Astron. Astrophys.*, *557*, A33, doi:10.1051/0004-6361/201322020.

Somogyi, A., K. Gringauz, K. Szego, L. Szabo, G. Kozma, A. Remizov, J. Ero, I. Klimenko, I. Szucs, M. Verigin, J. Windberg, T. Cravens, A. Dyachkov, G. Erdos, M. Farago, T. Gombosi, K. Kecskemety, E. Keppler, T. Kovacs, A. Kondor, Y. Logachev, L. Lohonyai, R. Marsden, R. Redl, A. Richter, V. Stolpovskii, J. Szabo, I. Szentpetery, A. Szepesvary, M. Tatrallyay, A. Varga, G. Vladimirova, K. Wenzel, and A. Zarandy (1986), 1st observations of energetic particles near comet Halley, *Nature*, *321*(6067), 285–288, doi:10.1038/321285a0.

Staines, K., A. Balogh, S. Cowley, R. Hynds, T. Yates, I. Richardson, T. Sanderson, K.-P. Wenzel, D. McComas, and B. Tsurutani (1991), Cometary water-group ions in the region surrounding comet Giacobini-Zinner: Distribution functions and bulk parameter estimates, *Planet. Space Sci.*, *39*, 479 – 506, doi:10.1016/0032-0633(91)90008-X.

Strobel, D. F. (2002), Aeronomic systems on planets, moons, and comets, in *ATmospheres in the Solar System: Comparative Aeronomy*, *Geophysical Monograph Series*, vol. 130, edited by M. Mendillo, A. Nagy, and J. H. Waite, pp. 7–22, AGU, WASHINGTON, DC 20009 USA, doi:10.1029/130GM02.

Szegő, K., K. Glassmeier, R. Bingham, A. Bogdanov, C. Fischer, G. Haerendel, A. Brinca, T. Cravens, E. Dubinin, K. Sauer, L. Fisk, T. Gombosi, N. Schwadron, P. Isenberg, M. Lee, C. Mazelle, E. Mobius, U. Motschmann, V. Shapiro, B. Tsurutani, and G. Zank (2000), Physics of mass loaded plasmas, *Space Sci. Rev.*, *94*, 429–671, doi:10.1023/A:1026568530975.

Tenishev, V., M. Combi, and B. Davidsson (2008), A global kinetic model for cometary comae: The evolution of the coma of the Rosetta target comet Churyumov-Gerasimenko throughout the mission, *Astrophys. J.*, *685*(1), 659–677.

Tsurutani, B. T. (1991), Comets: A laboratory for plasma waves and instabilities, in *Cometary Plasma Processes*, *AGU Geophysical Monograph Series*, vol. 61, edited by A. D. Johnstone, pp. 189–209, American Geophysical Union, doi:10.1029/GM061p0189.

Whipple, F. L. (1950), The acceleration of Comet Encke, *Astrophys. J.*, *111*, 375.

Wiehle, S., U. Motschmann, N. Gortsas, K. Glassmeier, J. Mueller, and C. Koenders (2011), Simulation of cometary jets in interaction with the solar wind, *Adv. Space Res.*, *48*(6), 1108–1113, doi:{10.1016/j.asr.2011.05.024}.

Young, D., F. Crary, J. Nordholt, F. Bagenal, D. Boice, J. Burch, A. Eviatar, R. Goldstein, J. Hanley, D. Lawrence, D. McComas, R. Meier, D. Reisenfeld, K. Sauer, and R. Wiens (2004), Solar wind interactions with comet 19P/Borrelly, *Icarus*, *167*, 80–88, doi: 10.1016/j.icarus.2003.09.011.

Zakharov, V. V., A. V. Rodionov, G. A. Lukianov, and J. F. Crifo (2009), Monte-Carlo and multifluid modelling of the circumnuclear dust coma II. Aspherical-homogeneous, and spherical-inhomogeneous nuclei, *Icarus*, *201*, 358–380, doi:10.1016/j.icarus.2008.12.022.

Corresponding author: Tamas I. Gombosi, Department of Atmospheric, Oceanic and Space Sciences, University of Michigan, 2428 Space Research Building, Ann Arbor, MI 48109, USA. (tamas@umich.edu)